6-1-2017 12:00 AM

Characterizing the Cofactor Specificity of NQO2

Shahed Al Massri, *The University of Western Ontario*

Supervisor: Dr. Brian Shilton, *The University of Western Ontario*
A thesis submitted in partial fulfillment of the requirements for the Master of Science degree in Biochemistry
© Shahed Al Massri 2017

Abstract

Quinone Reductase 2 (NQO2) is a part of an enzyme family implicated in detoxification of the cell. This enzyme differs from its highly similar sister protein Quinone Reductase 1 (NQO1) by its unique cofactor preference for dihydro-nicotinamide riboside (NRH) instead of NADH. Cellular levels of NRH have not been characterized, contributing to the mystery surrounding the physiological role of NQO2. This project focused on identifying what determines the cofactor specificity of NQO2, and engineering it to use NADH instead of NRH. The investigation included optimization of protein purification, an *in silico* analysis that revealed the different stereochemistry of NQO2/1 from other flavoenzymes, and an x-ray analysis of crystallized NQO2 after NADH soak. An informed site-directed mutagenesis approach yielded a 70-fold increase in the catalytic efficiency of NQO2 utilizing NADH, compared to the wildtype. The results of this project help characterize the cofactor preference of NQO2 on a molecular level.

Keywords

NQO2, NQO1, quinone reductase 2, quinone reductase 1, NRH, NADH, NADPH, NAD, NR, flavoprotein, quinone oxidoreductase, flavoenzyme, enzyme kinetics, x-ray crystallography, cofactor specificity, site-directed mutagenesis

Co-Authorship Statement

Phylogenetic tree (**Figure 6**) generously calculated by Dr. Brian Shilton. Refinement of NQO2 crystal structure with nicotinamide and **Figure 22** generously created by Kevin Leung of Dr. Brian Shilton's lab. Growing and soaking of the crystals, collection of data and initial refinement performed by Shahed Al Massri with the help of Dr. Brian Shilton and Kevin Leung. All other experiments and procedures described were performed by Shahed Al Massri.

Acknowledgments

First and foremost I would like to thank Dr. Brian Shilton for his mentorship and guidance through this project, as I have learned an incredible amount in the field of Biochemistry during my time here. Developing skills in performing research, gathering data, lab techniques and analytical thinking made pursuing this Master's degree an excellent decision for me, and it would not have been possible without his supervision.

I would like to thank my committee members Dr. Ball and Dr. Heinemann for their invaluable advice and wisdom on how to conduct my research and put together a well-rounded story. Their experience was humbling and extremely helpful.

I would like to thank Kevin Leung for his dedication to teaching me everything I had questions about. His patience, advice and commitment to making sure my learning experience was fruitful meant so much to me. I cannot thank him enough for how much advice he has given me.

I would like to thank Aliakbar Yazdi for sharing his knowledge in advanced lab techniques and research methods. He challenged the way that I think and approach things in a way that helped me grow as a student of science immensely, and I am really grateful for the experience.

Thank you to Joel Bierer, Laura Craven, Atif Nehvi, Wen Qin and Derek Tse for not only being wonderful peers to share and discuss our results with but also being a great source of laughs and good times in the lab. Thank you for some of the fondest memories of my time here.

Thank you to my family and friends for their words of encouragement through this herculean task, I appreciate your cheering me on more than you can imagine.

I dedicate this thesis to Mohamed, whose emotional support for me was unparalleled through the difficulties of this project, and impossible to put into words how much I am grateful for it. From the bottom of my heart: thank you for everything.

Table of Contents

List of Tables

List of Figures

List of Appendices

List of Abbreviations

QR – Quinone reductase

NQO1 – NAD(P)H:Quinone Oxidoreductase 1

NQO2 – N-ribosyldihydronicotinamide:quinone reductase 2

NADH – Dihydro-nicotinamide adenine dinucleotide

NAD – Nicotinamide adenine dinucleotide

NRH – Dihydro-nicotinamide riboside

NR – Nicotinamide riboside

MTT – 3-(4,5-dimethylthiazol-2-yl)-2,5-diphenyltetrazolium bromide

DMSO – Dimethyl sulfoxide

Chapter 1 – Introduction

Mapping out a protein's role in the cell is a very exciting process of research, and there are many proteins with yet undiscovered function in human cells. This project's overarching goal was to characterize the cofactor specificity of NQO2, a member of a protein family called quinone reductases, in order to help shed some light on its physiological role in the cell. The main purpose of this protein was thought to be detoxification of the cell through quinone reduction; however recent discoveries suggest that NQO2 may serve a signaling function beyond its redox mechanism. This hypothesis came about in part due to the fact that NQO2 uses a unique cofactor as an electron donor, dihydro-nicotinamide riboside (NRH), which is not utilized by any other proteins including related quinone reductase isoforms. This unique cofactor preference is a double-edged sword, suggesting the possibility of a signaling role for NQO2 but also being a source of difficulty in studying its *in vivo* contributions. In this research project, I have used a molecular-based approach to examine the cofactor specificity of NQO2 towards NRH as a stepping stone towards discovering its cellular role beyond the reduction of quinone compounds.

1.1 Quinones and quinone reductases

1.1.1 Quinones

Quinones are cyclic conjugated organic compounds abundantly found in living cells, serving a variety of functions such as electron acceptors and cofactors in protein mechanisms. Despite their importance in the cell, they are prone to forming radical intermediates named

semi-quinones, which are produced through a one-electron reduction (**Figure 1**). Semi-quinones can be formed spontaneously or through one-electron reductases (1). These radicals are highly unstable, and can react with oxygen to form superoxide species that are extremely reactive and therefore damaging to the cell. Quinone reductases prevent the formation of these harmful radicals by regulating the abundance of quinones through performing a two-electron reduction on them (2), resulting in the fully reduced hydroquinone form that is much less prone to auto-oxidation (3). This mechanism is the reason quinone reductases are considered members of the detoxification infrastructure that protects the cell from oxidative stress. It is believed that quinones existed in the environment and unicellular organisms from a very ancient time – as far as 2 billion years ago – which is why the QR family is also believed to be similarly ancient (4). There was likely strong selection pressure for an enzyme that prevents cellular damage from semi-quinone formation.
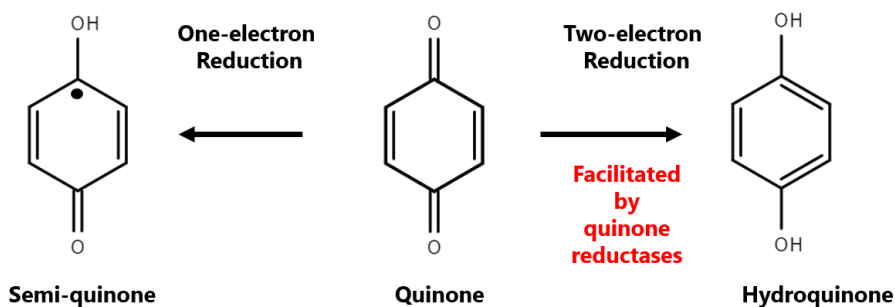
Figure 1: A two-electron reduction versus a one-electron reduction of quinones.

A one electron reduction results in the radical intermediate semi-quinone, while a two-electron reduction catalyzed by quinone reductases results in hydroquinone.

1.1.2 Quinone reductases

Quinone reductases (QRs) are a family of proteins ubiquitously found in both prokaryotic and eukaryotic cells. The earliest identified forms of QRs were originally dubbed

DT-diaphorases, stemming from their ability to utilize both NADH and NADPH as cofactors (1). The first QR was identified in rat liver, and is now referred to as NQO1. The "NQO" nomenclature is usually used for the vertebrate isoforms of these proteins, and they are expressed in varying levels amongst different tissues. One of the key characteristics of quinone reductases is a tightly-linked flavin molecule, which is critical for electron movement from cofactor to substrate in the reduction mechanism utilized by QRs (5). In the case of the vertebrate isoforms (NQO1, NQO2) this co-enzyme is flavin adenine dinucleotide (FAD), while in most other species (e.g. bacterial, yeast) it is flavin mononucleotide (FMN). With the exception of a few protein variants in plants and fungi, quinone reductases use a ping-pong mechanism to transfer two electrons from their respective nicotinamide cofactor (NADH, NADPH, NRH) to the flavin co-enzyme present in the protein. Once this occurs, the oxidized cofactor dissociates and the electrons are donated from the reduced flavin to the newly bound quinone substrate, thus concluding the ping-pong reduction mechanism.

QRs exist in dimeric or tetrameric forms. The mammalian isoforms of NQO1 and NQO2 are dimers. FAD molecules (one for each catalytic site) are non-covalently bound at the interface of the two monomers, situated at the bottom of an intermolecular cavity that serves as the catalytic site (**Figure 2**). There are several inter-molecular interactions (H-bonds, salt bridges) between the two monomers at the interface that offer great stability to the dimer, with a total interface area of ~2,700 $Å^2$ in NQO1 (6). The two catalytic sites in QRs are identical, and accommodate both the electron-donating cofactor and the electron-accepting substrate at different stages of the reduction mechanism. Residues from both monomer chains participate in the binding and enzymatic process at each catalytic site.
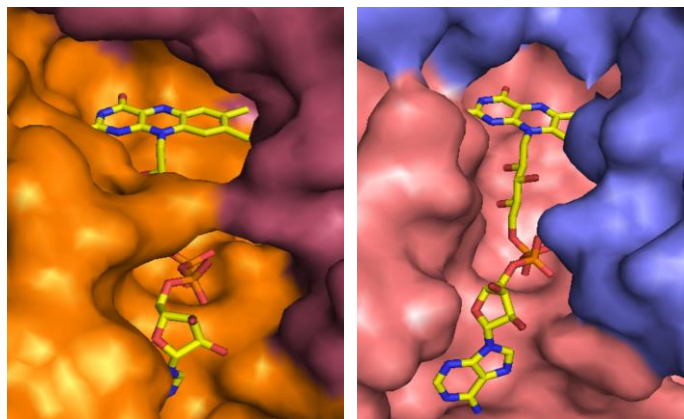
Figure 2: Catalytic sites in NQO1 and NQO2.

The NQO2 (left) and NQO1 (right) catalytic site cavities at the dimer interface, visualized by a surface representation of the crystal structures 1QR2 (NQO2) and 1D4A (NQO1) (7, 8). FAD molecule shown in yellow carbons. The monomeric units in each dimeric protein are highlighted in different colours. The bridge appearing over the FAD molecule in proximity to the catalytic cavity in NQO2 (left) is created by a hydrogen bond between the residues E193 and N66. Visualized in PyMOL (9).

1.2   A comparison of the similarities and differences between NQO1 and NQO2

The regulation and direct role of NQO2 in the cell have not been characterized as well as the sister protein NQO1. For this reason, a comparison between the two proteins is informative for elucidating the involvement of NQO2 in cellular functions. It is quite interesting that two sister proteins that share high structural, sequence, and mechanism similarity will reduce distinctly different cofactors and substrates. The role of NQO1 as a cytoprotective enzyme has been strongly supported through: the wide variety of chemicals that induce its activity, the fact that raising/lowering the protein's levels was associated with respectively decreased/increased susceptibility of the cell to oxidative stress, and its regulation through the Keap1/Nrf2/ARE pathway alongside other detoxifying genes (10).

On the other hand, there is limited knowledge of the regulation of NQO2 and the identity of its endogenous substrates in the cell. Comparing the similarities and differences between NQO2 and NQO1 was important for this project, as the differences between them were used to inform the approach for characterizing the unique cofactor preference of NQO2.

1.2.1   Similarities between NQO1 and NQO2

"NQO1" and "NQO2" hereafter refer to their mammalian isoforms within the quinone reductase family of enzymes. They are both dimeric, cytosolic proteins that are ubiquitously expressed in mammalian tissue, and their subunits are 274 and 231 residues in length respectively (11). Their subunit molecular weights are 30,880 and 25,956 Da respectively. The structures of NQO1 and NQO2 are highly similar **(Figure 3)**; as would be expected with 46% identity between the two sequences (**Figure A- 1, Appendix A).** A structural alignment in PyMOL reports an RMSD of 0.808 Å between the backbones of NQO2 and NQO1, which indicates high structural similarity between the two proteins. Both proteins contain a tightly-linked FAD molecule in each active site, which accepts electrons from their respective cofactors and subsequently reduce the substrate molecule.

Interestingly, there is strong evidence to suggest that NQO1 and NQO2 are involved in the p53 apoptosis signaling pathway of the cell (12, 13). For example, NQO2 was found to be the only human protein target of the antimalarial drug chloroquine, and chloroquine has been shown to activate the p53 pathway, but the process through which this occurs is unknown (14, 15). This led to the hypothesis that NQO2 is at least partially responsible for the off-target effects of chloroquine on p53 activation, and that NQO2 is involved in apoptosis signaling (see also **section 1.6**). Although the specific pathways by which these proteins are influencing p53

5

have not been characterized, there is accumulating evidence suggesting their involvement. The fact that these enzymes may serve an important cell signaling role beyond their detoxification task would be unusual, which is the reason they became the focus of this project. Characterizing their involvement in the p53 pathway would be highly intriguing due to the importance of p53 in apoptosis and tumor suppression.

1.2.2　Differences between NQO1 and NQO2

Although NQO1 and NQO2 share many similarities, they are specific to different cofactors, substrates, and are targeted by different inhibitors. Inhibitors of NQO1 such as phenindione, dicoumarol and Cibacron Blue do not inhibit NQO2 (16). Unique inhibitors of NQO2 include chloroquine, quinacrine, primaquine and resveratrol (14, 17).

The difference between NQO1 and NQO2 that is most relevant for this project is the cofactor used in their reduction mechanism. NQO1 can use either NADH or NADPH as an electron donor (18). In the case of NQO2, it uses reduced nicotinamide riboside (NRH) (**Figure 4**). There is a great deal of mystery surrounding NRH and its role in the cell, as NQO2 is the only enzyme known to utilize it as a cofactor (19). It is hypothesized to be a breakdown product of NADH because it has been observed in tissue extracts (20), but the cellular conditions which induce formation of NRH are unknown. It is worth noting that noticeable amounts of its oxidized form (NR) were observed in rat liver to arise from the enzymatic breakdown of NAD and NADP, the oxidized forms of NADH and NADPH (21).

The most noticeable structural difference between NQO1 and NQO2 is the presence of a flexible 43-residue C-terminal tail in NQO1 (**Figure 3**). This is considered a unique feature to NQO1 since it is not found in any other quinone reductase family members, such as the

bacterial and yeast isoforms. Originally this C-terminal tail did not resemble any known domains and was considered non-catalytic (5). However, upon removal of this C-terminal domain it was reported that the catalytic efficiency of NQO1 decreased from 440 to 1.2 min^{-1} µM^{-1}, suggesting that it serves an important role in the mechanism of NQO1 (22, 23). Interestingly the presence of this tail does not correlate with the enzyme preference to NAD(P)H versus NRH, for example the yeast isoform Lot6p and the bacterial isoform AcpD do not contain this C-terminal portion but still primarily utilize NADH/NADPH (24). The C-terminal tail was hypothesized to be partially responsible for NAD(P)H binding stabilization in NQO1 due to an observed interaction of Phe-232 in the tail with bound NADPH (25).
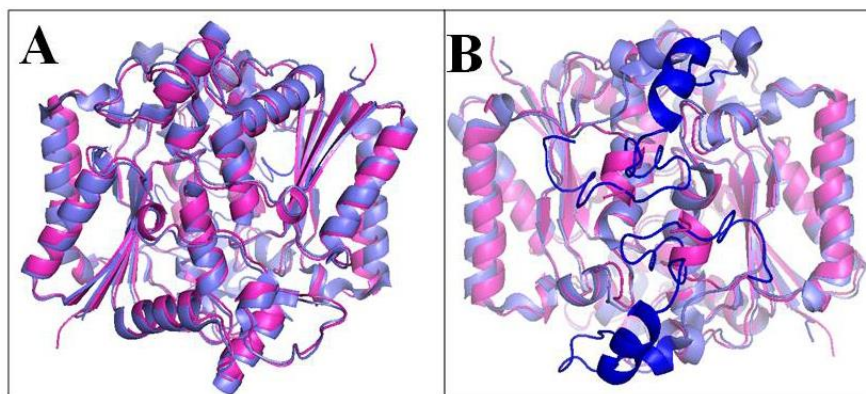
Figure 3: Superimposed cartoon representation of the backbones of NQO1 and NQO2.

NQO1 is shown in blue, while NQO2 is in magenta**.** Panels A and B show the protein from two different sides, rotated 180°. One of the main differences in the two proteins' structures is the presence of 43-residue C-terminal in NQO1, which is not present in NQO2. This C-terminal tail can be seen in Panel B, highlighted in dark blue.

While NQO2 has a much higher affinity for NRH over NADH, it has been observed to utilize NADH weakly as a cofactor, and the same for NQO1 utilizing NRH (23). The fact that NQO2 is capable of binding NADH in a productive manner was another important point to consider for this project, since the goal was to shift its cofactor specificity from NRH to NADH.
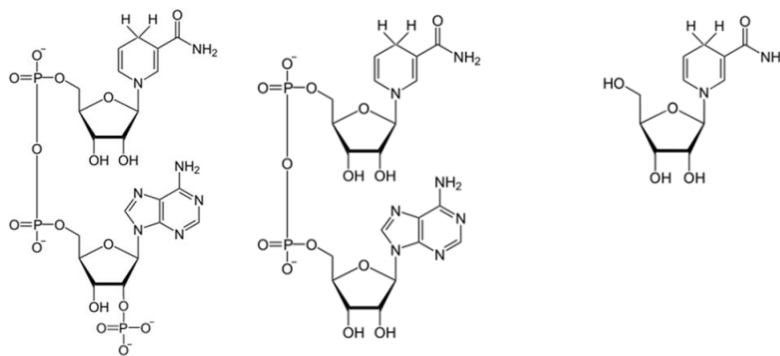
Figure 4: Structures of NADPH, NADH and NRH.

NADPH (left) and NADH (middle) are cofactors used by NQO1. NRH (right) is used by NQO2.

The kinetic parameters previously reported by Chen *et al.* for the two proteins with each cofactor are listed in **Table 1**. In a previous attempt to change the specificity of NQO2 to NADH (and NQO1 to NRH), a tail-less NQO1 as well as a chimeric NQO2 with the tail added were created (23). These modified proteins were assayed to determine whether the tail is responsible for the specificity of each protein towards their respective cofactors. The kinetics results showed that NQO1 functions significantly worse without its C-terminal tail, reporting a 300-fold decrease in catalytic efficiency using NADH, and a 20-fold decrease in its (already poor) efficiency using NRH. However, the results showed that removal/addition of the tail did not cause significant change in either protein's cofactor preference. This eliminates the possibility that the tail is responsible for the proteins' selectivity towards their respective cofactors, and suggests that there are more subtle elements at hand. It is not surprising that the C-terminal tail in NQO1 is not solely responsible for its preference towards NAD(P)H over NRH, since other NQO1 isoforms utilizing the same cofactor do not possess this tail region. However, the work done by Chen *et al.* (23) provides an excellent background for this project

since we were able to focus our attention on the NQO2 active site itself without having to consider whether the tail portion is partially responsible for the enzymes' cofactor preference.

Table 1: Previously published kinetic parameters for NQO1 and NQO2, using NRH or NADH as a cofactor

Kinetic paramaters for NQO2		
	NRH	NADH
K_m (µM)	28	330
k_{cat} (min^{-1})	2700	35
k_{cat} /K_m (min^{-1}µM^{-1})	96	0.1

Kinetic paramaters for NQO1		
	NRH	NADH
K_m (µM)	440	70
k_{cat} (min^{-1})	1680	30,900
k_{cat} /K_m (min^{-1}µM^{-1})	3.8	440

*Kinetic data in this table is reported from work by Chen *et al.* (23)

NQO2 contains one surface zinc binding site per monomer, which NQO1 does not possess (7). This zinc binding site exists approximately 10 Å from the active site. Past research shows that addition of zinc or copper (1 mM) did not have an effect on the activity of NQO2 (26). In addition, extensive dialysis of NQO2 against 100 mM EDTA as well as addition of 100 mM EDTA into the reaction solution did not significantly affect NQO2 activity, suggesting that the metal is not required for the enzyme's catalytic function (26). Some bacterial isoforms as well as common ancestors of NQO1 and NQO2 also possess this zinc binding site, but they do not share the specificity of NQO2 towards NRH.

The NQO1 and NQO2 active sites are quite similar with the exception of a few residues. A visualization of the surface of the two protein's active sites shows that the region around the binding cavity appears more restricted in NQO2, largely due to a hydrogen bond between E193

and N66 that forms a "bridge" over the FAD molecule (**Figure 2**). On the other hand, the differences in residues within the active site itself (directly above the isoalloxazine ring structure of the FAD molecule) result in a slightly larger and more hydrophobic binding pocket in NQO2 compared to NQO1 (5).

1.3   Reaction mechanism of NQO1 and NQO2
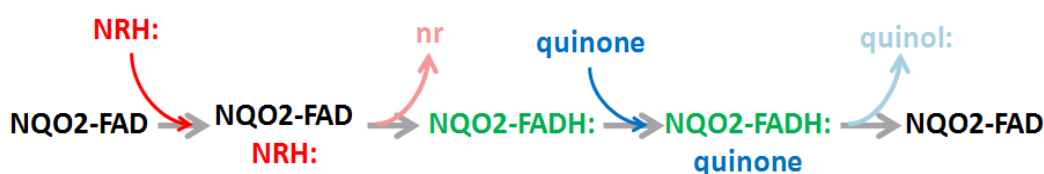
Figure 5: The ping-pong reaction mechanism of NQO1 and NQO2.

Two electrons are transferred from NRH to FAD, reducing it to $FADH_2$ and changing the overall protein's conformation to its reduced form (highlighted in green). The reduced NQO2-FADH complex can reduce quinones by transferal of two electrons. In the case of NQO1, NRH is replaced by NAD(P)H, which is oxidized to NAD(P).

Both proteins perform their reduction through a similar ping-pong mechanism (**Figure 5**). For NQO2, an NRH molecule will bind the active site and donate two electrons to the FAD molecule, reducing it to $FADH_2$. In previous work determining the reduced conformation of the enzyme, it was observed that the isoalloxazine ring of FAD acquires a 4-5° bend upon reduction, changing the overall conformation of the enzyme alongside it (19). This new conformation is hereafter referred to as the "active" or "reduced" form of NQO2, which is assumed to be an intermediate conformation of the protein upon receiving electrons from the cofactor. Once NR dissociates from the binding site, the enzyme can bind and reduce its quinone substrate to a hydroquinone (also referred to as quinol) and once again return to its oxidized form. This mechanism is the same in NQO1, with the exception of utilizing NADH or

10

NADPH instead of NRH. NQO1 does not significantly discriminate between NADH and NADPH; the rates of NQO1 reduction by NADPH and NADH were reported to be 11.3 x 10^8 and 8.8 x 10^8 M^{-1} min^{-1} respectively (27).

1.4   NQO1 and NQO2 knockout experiments

Knocking out a protein of interest can be quite useful in elucidating its physiological role in the cell. Any subsequent changes in the cell's phenotype can indicate which cellular processes the protein participates in. There have been several knockout experiments performed on quinone reductases, which have not conclusively demonstrated the processes NQO2 is involved in, but are important to consider for furthering the characterization of its role in the cell.

The yeast isoform Lot6p shares 21% sequence identity with NQO1, with a similar structure and quinone reduction mechanism utilizing NAD(P)H as a cofactor (5). Quinone reductases have been proposed to participate in the oxidative stress response, hence the effects of Lot6p knockout and overexpression were monitored under hydrogen peroxide-induced apoptosis (28). It was shown that Lot6p knock-out strains had a deficiency in apoptotic cell death compared to the wildtype, while overexpression resulted in enhanced levels of cell death. This implies a direct involvement of Lot6p in apoptotic cell death caused by oxidative stress in yeast.

When NQO1 or NQO2 was knocked out in mice, no effects on birth and reproduction were observed (29). However, the NQO2-knockout mice exhibited myeloid hyperplasia in their bone marrow. NQO1 deficient mice were more sensitive to hepatic toxicity induced by menadione than the wildtype, suggesting that NQO1 helps protect against menadione toxicity (30). Menadione (vitamin K3) is a quinone compound which is a substrate for both NQO2 and NQO1. NQO2 deficient mice on the other hand were less sensitive to menadione's effects,

11

suggesting that NQO2 plays a role in activation of menadione toxicity (11). In contrast, by comparing cells overexpressing NQO2 with wildtype and NQO2-deficient cells, it was found that NQO2 is an activator of the quinones Mitomycin C and BP-3,6-Q, and the anti-tumor drug CB1954 (31). This was reinforced by the fact that the cellular toxicity of these drugs was significantly higher in the presence of NRH in the medium, which is required for NQO2 activity.

In an experiment to investigate the role of NQO2 in protection against radiation-triggered oxidative stress, NQO2-knockout mice were shown to have higher susceptibility to myeloproliferative diseases induced by γ-radiation (32). NQO2 was shown to participate in protection against γ-radiation by preventing the degradation of myeloid differentiation factors by the 20S proteosome. The transcription factor C/EBPα is crucial for differentiation of immature granulocytes, and possesses a recognition sequence for degradation by the 20S proteasome. The study found that NQO2 competes with the 20S proteasome for that same binding sequence, thus protecting C/EBPα from degradation. Upon exposure of the mice to γ-radiation, NQO2 abundance and activity rose higher which led to decreased proteosomal degradation of C/EBPα and higher levels of NQO2 and C/EBPα interaction. These findings imply that NQO2 plays a significant role in prevention of some hematological disorders. This effect was shown to be independent of NQO1's presence in the cell.

It is worth noting that while the studies using NQO2-knockout mice showed that the mice exhibited myeloid hyperplasia (11) and increased susceptibility to certain carcinogens (29), other studies using imatinib treatments (found to be an off-target inhibitor of NQO2) did not observe these side-effects (33). The cellular function of NQO2 is yet to be fully deduced, considering that the origins and role of NRH in the cell remains a mystery.

One reason that knockout experiments with NQO2 are difficult to interpret for determining its physiological role is that the cellular conditions at which NRH is present are unknown. If it is unknown when NRH is available to allow NQO2 activity, it is difficult to determine the origin of the effects from knocking out the protein. This is one of the driving factors of this project, which aimed to create an NQO2 that uses the much better characterized NADH as a cofactor. If this was successful, the mutant NQO2 could be a significant boon for easier interpretation of the results of knockout experiments, in addition to helping characterize the cofactor preference of NQO2.

1.5   NQO1 and NQO2 common ancestry

A phylogenetic analysis of NQO1 and NQO2 revealed a common ancestor in ancient eubacteria which was dubbed 'NQO3' (4). We have used 33 different NQO homologs (4 bacterial ancestor NQO3 and 29 from NQO1/NQO2 isoforms found in vertebrates) to create a phylogenetic tree that illustrates the proteins' commen ancestry (**Figure 6**). This NQO3 nomenclature is not to be confused with the "NQO" prefix used for the vertebrate isoforms, but rather chosen to showcase that it is an evolutionary ancestor of these protein variants. These ancestral proteins are not fully characterized, but a few sequence-derived properties have been identified. NQO3 enzymes use NAD(P)H as a cofactor (34), which is interesting because it implies NQO2 diverged as an NRH-dependent protein likely due to evolutionary pressure towards fulfilling a task that the NADH-dependent quinone reductases did not serve. As for the 43-residue C-terminal tail found in NQO1, the NQO3 proteins did not include such a region. This property remains unique to NQO1, and suggests that it may serve a function that appears unrelated to the preference towards NAD(P)H. Some of the NQO3 sequences reveal a zinc-binding site, which is also found in NQO2 but not in NQO1.
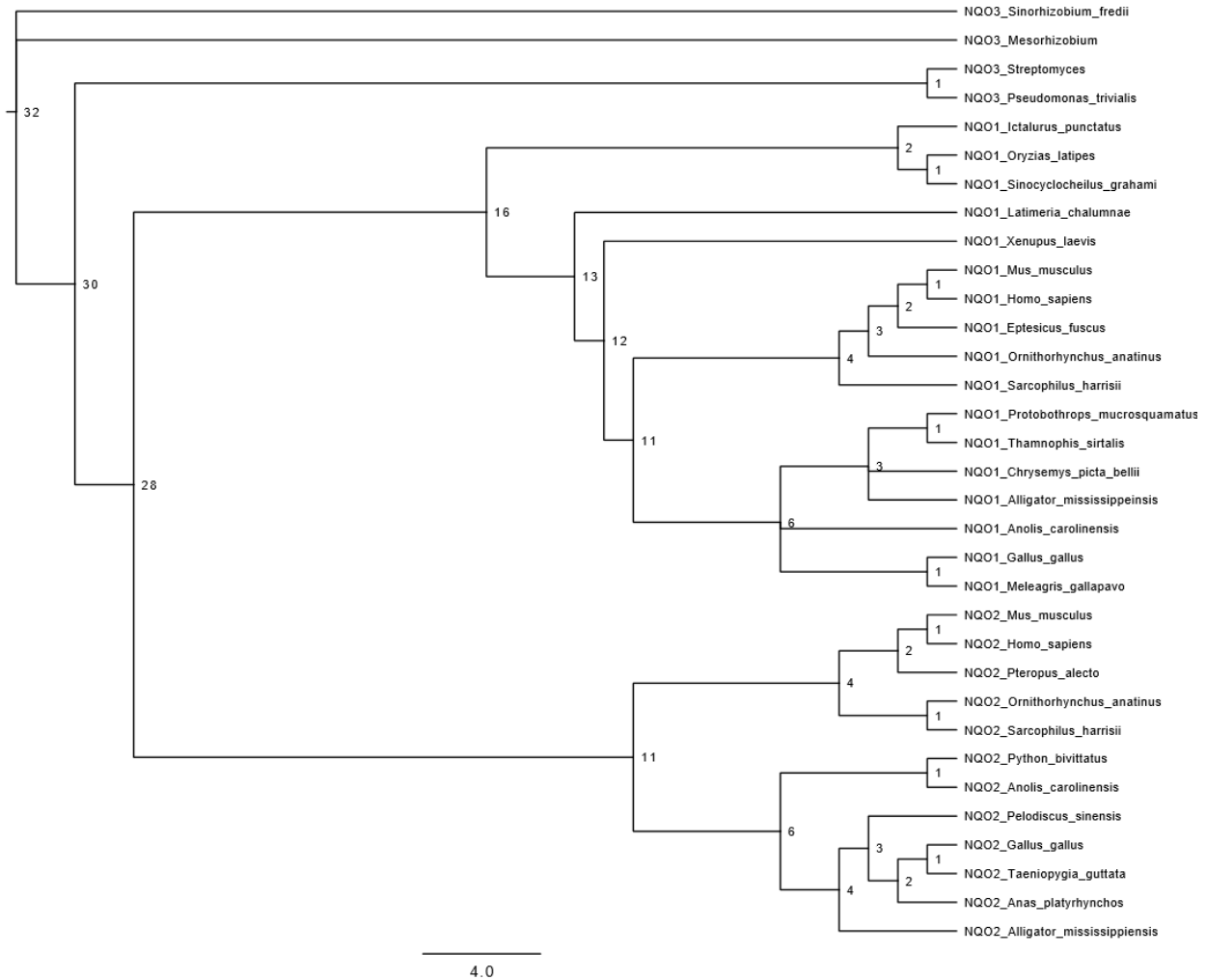
Figure 6: Phylogenetic tree showcasing NQO1 and NQO2 common ancestry.

Phylogenetic calculation in MrBayes and phylogeny.fr (35, 36) including 33 NQO sequences, four "NQO3" from eubacteria and the remainder sequences are from various NQO1/NQO2 isoforms found in vertebrates

1.6   Evidence towards the involvement of NQO1 and NQO2 in p53-signalling pathways

An interesting facet of both NQO1 and NQO2 is their possible connection to the

apoptosis signaling pathway of the cell through the transcription factor p53. NQO1 was shown

to be involved in the stabilization of p53 in an experiment where inhibition of NQO1 by

14

dicoumarol resulted in a decrease in p53 levels due to its degradation (12). It was observed that when NQO1 was overexpressed in colon carcinoma cells, p53 levels remained stable despite addition of dicoumarol. It was also observed that induction by oxidative stress resulted in the highest levels of NQO1-mediated stabilization of p53. These data strongly supports a role for NQO1 in apoptosis-signaling through stabilization of p53 against degradation.

Another connection between NQO1 and NQO2 and p53 activation was established in an experiment that measured accumulation of p53 due to exhaustion of pyrimidine nucleotides in the cell (13). It was previously known that p53 was activated by a mitochondrial signal from the electron transport chain (ETC), but the mechanism was unknown. By inhibiting different components of the ETC, it was found that p53 stabilization occurred when complex III inhibitors were used, resulting in depletion of pyrimidines in the cell. However, this effect was abrogated when NQO1 and NQO2 were removed using siRNA together with inhibition of complex III, implying that NQO1 and NQO2 play a key role in mitochondrial–induced stabilization of p53. NQO1 and NQO2 were also observed to co-localize with p53 from the cytoplasm to the nucleus. NQO1 and NQO2 are usually found in the cytoplasm, therefore it was unusual to observe them localizing elsewhere for a specific function.

Although the connection between NQO2 and p53 is yet to be fully elucidated, there is more evidence which points to a potential role in facilitating p53 activity. NQO2 was identified by a proteomic approach to be one of the two protein targets of the anti-malarial drug chloroquine, the other protein being aldehyde dehydrogenase 1 (14). Of the two proteins, NQO2 was found to be the only one significantly inhibited by concentrations of chloroquine used in clinical treatment. Chloroquine had previously been found to activate the p53 apoptosis pathway in

human glioblastoma cells (15). Since the drug inhibits NQO2, chloroquine's involvement in the p53 pathway suggests a connection between NQO2 and p53.

Chloroquine is used to treat diseases other than malaria, such as rheumatoid arthritis and is under investigation for use as a chemotherapy drug and to treat HIV-1/AIDS (37–39). Therefore, inhibition of NQO2 could be relevant in other types of diseases as well.

Since NRH may be a breakdown product of NAD(P)H, and NQO2 is hypothesized to serve an apoptosis-related signaling function through p53, it is possible that NRH serves as a signaling molecule for apoptosis through NQO2. Exploring this potential function is of great interest to us, and it is the reason why this project was designed to help elucidate the physiological response that the NRH-driven activity of NQO2 may elicit *in vivo.*

1.7   Project goals

This project focused on determining why NQO2 has a preference for NRH over NAD(P)H; uncovering the molecular determinants for this cofactor specificity. If reduction of NQO2 through NRH acts as a molecular switch for p53, *in vivo* studies examining the cellular effect of NQO2 might provide some insight on its role in the pathway, and the signaling role of NRH. Since the cellular conditions at which NRH is present are not yet understood, the results of induction or knockout experiments are difficult to interpret for determining the cellular role of NQO2.

Since the cellular abundance of NAD(P)H is well characterized (40–42), we speculate that engineering NQO2 to use NADH or NADPH instead may serve as a solution for elucidating its role in cell signaling. If the original function of the enzyme is retained in the

mutant NQO2, we predict that *in vivo* analysis of the physiological function of NQO2 would become significantly easier. For example, experiments involving knockout or elevated expression of NQO2 will be more conclusive, since the cellular levels of NAD(P)H are established and therefore it will be known when the mutant protein is active. Since the presence of the 43-residue C-terminal tail from NQO1 was not found to be responsible for either proteins' cofactor preference (23), this investigation took a more specific approach to altering the cofactor specificity of NQO2, using site-directed mutagenesis informed by the binding site of NQO1.

The molecular details of NRH binding within NQO2 (as well as NADH binding within NQO1) are unknown, which is the biggest obstacle for targeted mutagenesis aimed at changing its specificity to NRH. Based on the way NAD(P)H binds and donates electrons in other flavoenzymes, it was assumed that NRH binds NQO2 by similar stacking of the nicotinamide over the isoalloxazine ring of FAD. N4 in the nicotinamide moiety directly stacks onto N10 of the isoalloxazine ring of FAD, bringing the two reducing sites from each molecule in close proximity for the electron transfer to occur. This process is characteristic of flavoenzymes (43). However, since a crystal structure of NQO2 with bound NRH has not been obtained, the residues involved in binding/catalysis have not been identified. The crystal structures available for NQO2 are the native protein (PDB ID: 1QR2), and several structures of NQO2 bound to inhibitors.

It is important to note that although NQO2 has a preference for NRH, there is evidence that it can still utilize NADH as a reductant. The reverse is true for NQO1: it weakly utilizes NRH. In addition to the parameters obtained by Chen *et al.* (**Table 1**), it was observed that NQO2 metabolized the anti-tumor compound CB10-200 in the presence of 500 µM NADH,

also showing that NQO2 may be able to use NADH as a substrate to some extent (44). Another study also found that NQO2 can weakly utilize NADH, with a K_m of approximately 300 µM (45). Thus, the cofactor specificity of the two proteins is not absolute.

As previously mentioned, NQO1 does not readily discriminate between NADH and NADPH. If the cofactor specificity of NQO2 was successfully changed from NRH to NAD(P)H, similar affinities to both molecules may be observed. Cellular levels of NADH are usually low, with an NAD+/NADH ratio of 644 (41). On the other hand, relative NADPH levels are normally much higher, with an NADP+/NADPH ratio of about 0.01 (42) . Therefore determination and comparison of the affinities of the proposed mutant NQO2 for all three molecules is crucial.

Our overall investigation into the cofactor specificity of NQO2 would help pave the way for addressing two topics. One of them is to help answer the question of how NQO2 evolved to use NRH. The other is that if the proposed mutant NQO2 uses NAD(P)H preferentially over NRH but still retains the original function of NQO2, it would be highly useful for *in vivo* determination of the role of NQO2, since it would be known when the protein is active. Uncovering the cellular function of NQO2 would be a big step forward towards elucidating what NRH may signal about state of the cell that would elicit the signal for apoptosis.

Chapter 2 – Materials and Methods

FAD, bovine serum albumin (BSA), phenylmethanesulfonyl fluoride (PMSF), menadione, 3-(4,5-dimethylthiozol-2-yl)-2,5diphenyltetrazolium (MTT), reduced nicotinamide adenine dinucleotide (NADH) were purchased from Sigma-Aldrich. NaCl, Tris, HEPES, $(NH_4)_2SO_4$ and NaH_2PO_4 purchased from EMD chemicals. Ampicillin, lysozyme, dithiothreitol (DTT) were purchased from Bioshop Canada. Full length human NQO1 cDNA clone was purchased from OriGene. Protein concentrations were determined using a Bradford assay with a BSA standard. All SDS-PAGE gels were stained with solution containing 0.5 g/L Coomassie™ Brilliant Blue.

2.1 Cloning and site-directed mutagenesis

Mutations were introduced to NQO2 using the protocol for site-directed mutagenesis Quikchange™ by Stratagene (La Jolla, CA). The primers used are listed in **Table 2**. PProEx-HTa (Invitrogen) plasmid containing full-length His-tagged human NQO2 was used as the template for site-directed mutagenesis. The PCR products were transformed into XL1B *E. coli*, and incubated overnight on plates containing ampicillin (0.1 mg/mL) in order to select for transformants. Colonies were picked, followed by plasmid extraction and sequencing to confirm the presence of the desired mutations. The extracted plasmid was then transformed into BL21 *E. coli* and grown overnight for expression and purification of the protein.

Full-length human NQO1 cDNA clone (OriGene) was modified through mutagenic PCR to include restriction sites for *Nco*I and *Xba*I flanking the protein sequence, primers used are listed in **Table 3**. The primers allowed for an in-frame insertion of the protein sequence within the plasmid. The product was cloned into PProEx-HTa plasmid (also containing the

same restriction sites in its polylinker region) through digestion with *Nco*I and *Xba*I and subsequent ligation. The final construct includes a TEV protease cleavage site as well as a His-tag upstream of the protein sequence. The nucleotide sequence for NQO1 was verified within the construct by sequencing, then transformed into BL21 *E. coli* cells for protein expression.

Table 2: Primers used for site-directed mutagenesis of NQO2

Primer Name	Primer Sequence
a199c_t201g	5'-CTTTCTAATCCTGAGGTTTTCCAGTATGGAGTGGAAACCCACG-3'
a199c_t201g_antisense	5'-CGTGGGTTTCCACTCCATACTGGAAAACCTCAGGATTAGAAAG-3'
c217g_a218t	5'-CAATTATGGAGTGGAAACCGTCGAAGCCTACAAGCAAAGG-3'
c217g_a218t_antisense	5'-CCTTTGCTTGTAGGCTTCGACGGTTTCCACTCCATAATTG-3'
c367g_a368g	5'-GGATAGGGTGCTGTGCGGGGGCTTTGCCTTTGAC-3'
c367g_a368g_antisense	5'-GTCAAAGGCAAAGCCCCCGCACAGCACCCTATCC-3'
a385t_t386a_c387t	5'-CCAGGGCTTTGCCTTTGACTATCCAGGATTCTACGATTCCG-3'
a385t_t386a_c387t_antisense	5'-CGGAATCGTAGAATCCTGGATAGTCAAAGGCAAAGCCCTGG-3'
a581g_	5'-GATCAGCTTTGCTCCTGGAATTGCATCCGAAGAAG-3'
a581g_antisense	5'-CTTCTTCGGATGCAATTCCAGGAGCAAAGCTGATC-3'

Table 3: Primers used for addition of flanking restriction sites to NQO1 sequence

Forward primer (*Nco*I site)	5'-GAGCCATGGTCGGCAGAAG-3'
Reverse primer (*Xba*I site)	5'-GGCTCTAGATTATTATTTTCTAGCTTTGATCTGGTTGTC-3'

2.2 Protein expression and purification

2.2.1 Expression and purification of proteins

Recombinant human NQO2 and the mutant proteins were expressed and purified using previously described methods (46). NQO1 was also expressed and purified using the same methods.

BL21 *E. coli* cells transformed with the recombinant plasmid containing the respective His-tagged protein were grown in auto-induction media as described by Studier (47). Ampicillin (0.1 mg/mL) was included in the culture media in order to select for cells expressing the desired plasmid. The cell culture was incubated in four identical 1-litre media flasks for 19 hours at 37°C while shaking at 220 RPM. Cells were harvested by centrifuging at 6,000 RPM for 10 minutes in JLA-8.1 Rotor, and re-suspending the pellets in 50 mL of 50 mM phosphate buffer 500 mM NaCl pH 7.5. Harvested cells were flash frozen at - 80°C then thawed and lysed by French press the next day after addition of 1 mM PMSF. The cell lysate was applied to a 20 mL Ni^{2+}-bound Chelating Sepharose Fast Flow column, and NQO2 was eluted by raising imidazole concentration from 20 to 500 mM. After His-tag cleavage using tobacco etch virus (TEV) protease and 5 mM DTT, the protein was dialyzed overnight to decrease salt concentrations in preparation for anion exchange. The protein was applied to a 1.6 x 15-cm Q-Sepharose HP (GE Healthcare) anion exchange column and eluted with a NaCl gradient from 0 to 500 mM over a volume of 200 mL. The Q-Sepharose column was equilibrated with 50 mM Tris-HCl pH 8. NQO2 containing fractions were pooled and concentrated to a volume of 5 mL, and treated with guanidine-HCl and FAD to final concentrations of 3M and 10 µM respectively. Denaturation with guanidine-HCl and allowing it to refold in the presence of FAD during size exclusion chromatography was performed for the purpose of fully reconstituting the protein with FAD rather than FMN. A 2.6 x 65-cm Superdex 200 (GE healthcare) size-exclusion column was equilibrated with 50 mM Tris-HCl 150 mM NaCl 10 µM FAD pH 8, and the concentrated protein was applied and resolved at a flow rate of 2 mL/min. Full reconstitution of FAD within the purified proteins was confirmed through absorbance measurements at 273 and 450 nm according to previous methods (46).

2.2.2   Modification to purification protocol by DTT addition

A modification to the above purification protocol was the addition of 10 mM DTT into the guanidine-HCl denaturation step to prevent misfolding of the protein during the gel filtration. After incubating on ice for 5 minutes, the protein solution was applied to a Superdex-200 column equilibrated with 50 mM Tris-HCl 150 mM NaCl 10 µM FAD (pH 8.0). Fractions containing NQO2 were pooled, concentrated to 25 mg/mL, aliquoted, flash frozen and stored at -80 °C for crystallization and analysis.

2.3   Crystallization and diffraction data collection of NQO2 with NADH

Purified wildtype NQO2 at a concentration of 25 mg/mL was crystallized by hanging drop diffusion (drop volume of 1 µL) against reservoirs containing 0.1 M HEPES and concentrations of $(NH_4)_2SO_4$ ranging from 1.2-2.2 M, at pH 7, 7.5 and 8. NQO2 was co-crystallized with 10 mM NADH by mixing 0.5 µL of 20 mM NADH solution to 0.5 µL of concentrated protein into the tray well. Crystals were soaked for 1 minute in 2 µL of 20% glycerol, 2 M $(NH_4)_2SO_4$, 0.1 M HEPES pH 7.5 and 10 mM NADH, and the colour of the crystal was observed to change from yellow to clear. The crystal was then flash frozen and mounted for data collection.

Diffraction data were collected using a rotating anode source emitting X-rays at a wavelength of 1.5418 Å. Data were processed using MOSFLM (48) and merged using Scala-CCP4 (49). Protein structure was solved using molecular replacement with 1QR2 as the starting model. Data was refined using PHENIX (50).

2.4　Absorbance spectrum collection of NQO1, wildtype NQO2, triple mutant and quintuple mutant

Solutions of purified NQO1, wildtype NQO2, triple and quintuple mutant were diluted in Tris-HCl pH 8.0 and dialyzed using the same buffer. The solutions' final concentrations were measured by Bradford assay. After baseline correction using the dialysis buffer, an absorbance spectrum was measured from 250 to 500 nm in a Cary 100-Bio spectrophotometer (Varian). The obtained spectra were scaled to correspond to 1 mg/mL based on the concentrations determined by the Bradford assay.

2.5　CD Data collection

Circular dichroism scans were obtained using a Jasco J-810 spectropolarimeter. A cell with path length of 0.1 mm was filled with protein solution diluted with buffer (20 mM sodium phosphate, 100 mM NaCl, pH 7.5). The protein was dialyzed in the buffer prior to measurement, and the buffer used in the dialysis was used to blank the instrument. The exact concentration of each protein solution was measured by Bradford assay in triplicate. The scans were performed at 20° C at 0.5 nm intervals from 190 to 260 nm. The data were normalized into molar ellipticity (Θ_{MRE}) values using the concentrations obtained by the Bradford assays.

2.6　Thermal denaturation curves

Thermal denaturation scans were obtained using a Jasco J-810 spectropolarimeter. A cell with a volume of 300 µL and a path length of 1 mm was used for the measurements. The protein was dialyzed and diluted in the same buffer as the circular dichroism scans (above), and the protein concentrations were measured by Bradford assay. The scans were performed at 220

nm from 20° C to 90° C at a temperature increase rate of 1 degree per minute. The data were

normalized into molar ellipticity (Θ_{MRE}) values using the concentrations obtained by Bradford

assay. The data were fit to **Equation 1** with GraphPad Prism 4 software, using a linear

extrapolation method adapted from previous work (51, 52). In this equation, x is the

temperature in Kelvin, m_n and m_d are the slopes of the native and denatured baselines

(respectively) while y_d and y_n are the respective y-intercepts of those baselines. T_m is the

inflection point and represents the melting temperature at which the protein is 50% denatured.

R is the gas constant in units of kcal/mol•K, and ΔH_m is the enthalpy of unfolding at the T_m in

kcal/mol. This equation provides a calculation of the T_m from the data obtained in the thermal

denaturation assay as well as an analysis of the fit of the melting curves.

Equation 1: Linear extrapolation equation used for fitting thermal denaturation curves

$$y = \frac{(y_n + m_n x) + (y_d + m_d x) exp\left[\frac{\Delta H_m}{R}\left(\frac{1}{T_m} - \frac{1}{x}\right)\right]}{1 + exp\left[\frac{\Delta H_m}{R}\left(\frac{1}{T_m} - \frac{1}{x}\right)\right]}$$

2.7   Enzyme kinetics using NADH as a cofactor

Enzyme kinetics were obtained using a Cary 100-Bio spectrophotometer (Varian).

Measurements were done under stirring in a 4.5 mL cuvette with a final volume of 2 mL. The

components of the reaction solution were enzyme (NQO1, wildtype NQO2, triple mutant or

quintuple mutant), menadione, MTT, NADH and Tris-HCl pH 8 buffer. MTT and menadione

concentrations were kept constant in each reaction at 241 µM and 10 µM respectively. The

reaction was monitored at 610 nm following addition of enzyme. Reduced menadione will

reduce MTT in a non-catalyzed reaction, thus a change in absorbance corresponds to change in

levels of reduced MTT which indicates the enzymatic rate of menadione turnover using NADH as a cofactor. The reactions were performed at 20 °C. An MTT extinction coefficient of 11.3 x 10^3 M^{-1} cm^{-1} was used to convert the rate of change in absorbance into moles of menadione reduced per minute.

Chapter 3 – Results

3.1   Introduction

The main goal of this project is to ultimately shed some light on why NQO2 has a preference for NRH over NAD(P)H. Since the sister protein NQO1 as well as other flavoenzymes (FAD-dependent oxidoreductases) typically utilize NADH and/or NADPH as electron donors, the goal was to identify the factors which determine the cofactor specificity of NQO2 for NRH over NAD(P)H. The first line of thought would be that NAD(P)H is a bigger molecule than NRH and is unable to bind within the active site of NQO2 due to steric hindrance. However; past research has shown that NQO2 can weakly utilize NADH (**Table 1**). This implies that NAD(P)H binding is possible within NQO2. Considering the fact that the two enzymes' active sites are highly similar, the factors that determine its preference for NRH are likely subtle. By attempting to shift the cofactor specificity of NQO2 to NAD(P)H using site-directed mutagenesis, I hope to not only address the molecular factors that give NQO2 this unique preference, but also generate a mutant NQO2 that could be utilized in future *in vivo* studies investigating the protein's signaling role. A mutant NQO2 that utilizes NAD(P)H instead of NRH could be highly useful for such studies, as the cellular levels of NAD(P)H are much better characterized.

The molecular details of NRH binding within NQO2 (as well as NADH binding within NQO1) are unknown, creating an obstacle for targeted mutagenesis aimed at changing its specificity to NRH. Based on the way NAD(P)H binds and donates electrons in other flavoenzymes, it is assumed that NRH binds NQO2 by similar stacking of the nicotinamide over the isoalloxazine ring of FAD. However, the residues involved in binding/catalysis are not

known, as a crystal structure with bound NRH has not been obtained. The sister protein NQO1, which shares 46% sequence identity with NQO2, is a great resource for a site-directed approach to modify the specificity of NQO2 without knowing the exact molecular aspects of binding. The fact that NQO1 utilizes NAD(P)H despite sharing high structural similarity with NQO2 implies that the determinants of their specificity are subtle, and can be feasibly identified through site-directed mutagenesis. By directly comparing the active sites of the two proteins, I have chosen five different residues to mutate that significantly differ in their physicochemical properties.

3.2   Selecting the mutation sites, creating the mutants and characterizing their effects compared to wildtype NQO2 and NQO1

The target residues were mutated to the corresponding ones found in NQO1. A triple mutant dubbed NQO2-trp (Q122G, H72V, I128Y) and a quintuple mutant dubbed NQO2-qtp (Q122G, H72V, I128Y, E193G, N66Q) were constructed based on that comparison. The two mutants as well as wildtype NQO1 and NQO2 were expressed and purified from *E. coli,* followed by an assessment of their structural integrity using circular dichroism. Kinetic assays comparing the cofactor specificity of these two mutants to the wildtype will pave the way towards more specific analysis using single mutants to assay each residue's contribution to the observed change in cofactor specificity.

3.2.1   Superimposition of NQO2 and NQO1 active sites revealed potential targets for mutations

NQO1 and NQO2 share 46% identity in sequence, and are quite similar in their overall structure. In fact, the most major structural difference between them is the presence of a 43-

residue C-terminal tail in NQO1 that is not found in NQO2. In previous work, an NQO2 chimeric protein containing the C-terminal tail found in NQO1 was created in order to determine whether that feature was responsible for the difference in their cofactor preference (23). However, this did not yield a significant change in specificity. These findings led us to take a site-directed approach to engineer the protein's specificity by directly comparing the active sites of the two proteins.

A comparison of the active sites of NQO1 and NQO2 revealed that most of the residues are similar in their physicochemical properties, with a few exceptions. Through superimposition of the two proteins, I identified five different residues within the proteins' binding sites that are significantly different in size and/or charge between the two proteins (**Figure 7**).

The first two mutations (Q122G, H72V) were chosen due to their proximity to the binding site as well as the difference in size and charge (**Figure 7, left panel**). Since NADH is a larger molecule than NRH, it seemed possible that these residues are involved in steric hindrance that interferes with binding of NADH. The third mutation (I128Y) is the closest to the binding site of the nicotinamide ring, present on a flexible loop which closes down over the active site during binding (19). Its difference in size and aromaticity as well as its proximity to the binding site makes it worthy of investigation (**Figure 7, middle panel**). NADH has an additional aromatic ring compared to NRH due to its adenine moiety, and it is possible that the tyrosine residue in NQO1 promotes NADH binding through aromatic stacking. The last two mutations (E193G and N66Q) were chosen because these two residues participate in a hydrogen bond in close proximity to the active site, as seen by the fact that the distance between the two heavy atoms is 3.0 Å (**Figure 7, right panel**). Since this hydrogen bond is not found in NQO1, I hypothesized that these residues may make it more difficult to bind NADH in NQO2

due to steric hindrance and reduced flexibility of the protein backbone, shifting specificity to NRH which is a smaller molecule.
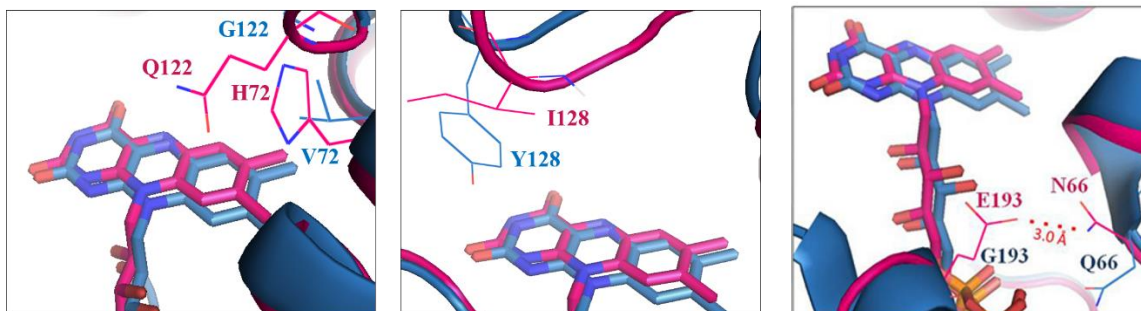
Figure 7: Target residues for mutagenesis in NQO2 active site chosen through superimposition with NQO1.

NQO2 (magenta carbon atoms) is superimposed with NQO1 (blue carbon atoms), with the five residues chosen for mutation labelled. In the right panel, asparagine and glutamic acid in NQO2 form a hydrogen bond (distance between the two heavy atoms is 3.0 Å) which is not found between the respective glutamine and glycine residues in NQO1.

The final mutant proteins contained multiple mutations in order to determine whether they result in a significant difference to the cofactor specificity of NQO2, paving the way for future analysis of each residue's individual contribution. Two mutant species were created, a triple mutant dubbed NQO2-trp containing Q122G, H72V, I128Y, and a quintuple mutant dubbed NQO2-qtp containing Q122G, H72V, I128Y, E193G and N66Q.

3.2.2   Site-directed mutagenesis of NQO2

The desired mutations were introduced to NQO2 using Quikchange™ site-directed mutagenesis protocol. PCR using mutagenic primers was performed in multiple rounds of single mutations in order to achieve the final mutant constructs. This ensured the creation of a vector library that contained single as well as various combinations of the mutations. The final

mutants can be initially analyzed for the mutations' effect in combination, and the single and double mutant vectors created can be used for future residue-by-residue analysis of their contribution to the observed effects in cofactor specificity. Since the chosen residues included E193 and N66 due to their participation in a hydrogen bond that was not observed in NQO1, these sites were deemed most likely to have a pronounced effect on enzyme stability and kinetics. Therefore, it was decided that the final products for analysis would be a triple mutant (excluding them) and a quintuple mutant (including them), in order to distinguish their effects from the rest of the mutations. The PCR product was transformed into *E. coli* strain XL1B, incubated overnight, then the plasmid was isolated and sequenced in order to ensure the presence of the desired mutations. The sequencing alignment showed that the triple (**Figure B-1, appendix B**) and quintuple (**Figure B- 2, appendix B**) mutants (NQO2-trp and NQO2-qtp) contained the correct substitutions.

3.2.3   Expression and purification of NQO1, NQO2 and mutants

3.2.3.1   Protein purification

This section describes the purification process and results for wildtype NQO2 in detail, as an example for NQO1, NQO2-trp and NQO2-qtp purification where the same protocol was used and similar yields were obtained. NQO1, NQO2, NQO2-trp and NQO2-qtp were expressed in *E. coli* strain BL21 as His-tagged constructs in plasmid PProEx-HTa using auto-induction media (47). The auto-induction media gave a high yield of cells, with an OD_{600} of approximately 10 upon exiting log phase. This corresponds to a cell concentration of 8.0 x 10^9 cells/ml. A sample of culture post-incubation showed high amounts of NQO2 expression in

SDS-PAGE (**Figure 8**). The large amounts of protein expressed contributed to high success of the subsequent purification steps, increasing the quality and yield of the final purified proteins.
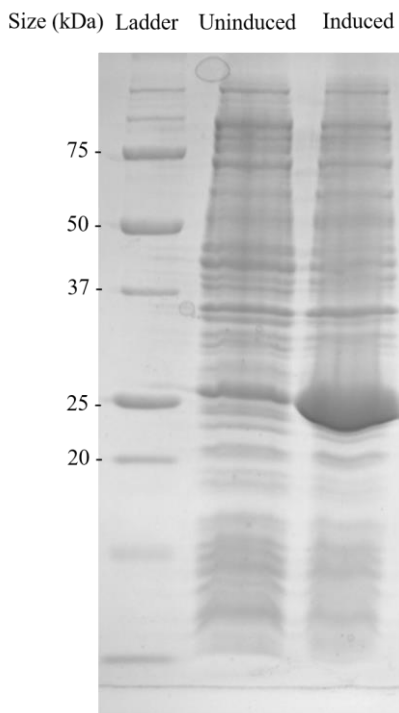
Figure 8: SDS-PAGE of expression of wildtype NQO2 in E. coli BL21 using auto-induction media.

NQO2 is 26 kDa in size. The second lane is a culture sample taken before incubation overnight in auto-induction media, representing the uninduced bacteria culture. The 3rd lane is a culture sample taken post-overnight incubation, showing the relative amount of NQO2 expressed

Cells were centrifuged and re-suspended in 50 mM sodium phosphate pH 7.5, lysed through French press and purified through nickel affinity chromatography. Each fraction was sampled and analyzed with SDS-PAGE (**Figure 9**). It appears that NQO2 was present in the flow-through and washes, suggesting that the column was overloaded with NQO2. Due to the relatively large amounts of expressed protein in the lysate, the purification quality was excellent perhaps due to the elimination of most non-specific binding to the column by sheer competition. Following nickel-column purification, the eluted protein was digested with TEV-

protease in the presence of 5 mM DTT. This was performed to cleave the His-tag from the protein in order to ensure its normal binding/folding/function during enzymatic assays. Digestion with TEV-protease leaves behind two residues at the N-terminus of the protein (glycine and alanine) which are not expected to hinder the structure and/or function of the protein. His-tag removal was tested by SDS-PAGE before/after digestion, showing that the product was approximately 1 kDa smaller (data not shown). The digested protein was dialyzed overnight into 50 mM Tris-HCl pH 8 in order to eliminate NaCl and imidazole in preparation for anion exchange chromatography.
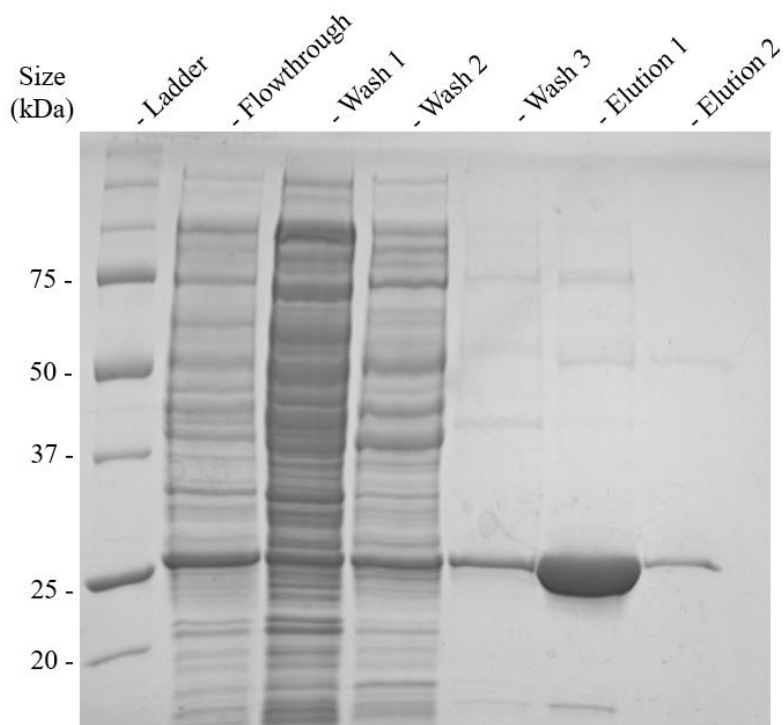
Figure 9: SDS-PAGE of nickel column purification of NQO2.

An SDS-PAGE of samples taken through the nickel column purification steps. Lane 2 is the flow-through of the lysed cells through the nickel column, lanes 3 through 5 are samples of column washes with 50 mM sodium phosphate 500 mM NaCl 20 mM imidazole pH 7. Lanes 6 and 7 are samples of subsequent elutions with 50 mM sodium phosphate 500 mM NaCl 500 mM imidazole pH 7.

Although purification quality following nickel column was acceptable, additional purification steps were performed in order to ensure highest purity for subsequent crystallization and enzymatic assays. The protein yield was large enough to allow some loss of protein in each step in favor of purification quality. Anion exchange was performed on the dialyzed, TEV-protease digested protein, with a NaCl concentration gradient of 0 to 500 mM.

The protein began eluting at approximately 25 mM NaCl over 13 fractions, each a volume of 8 mL. SDS-PAGE of the eluted fractions showed excellent purity (**Figure 10**).
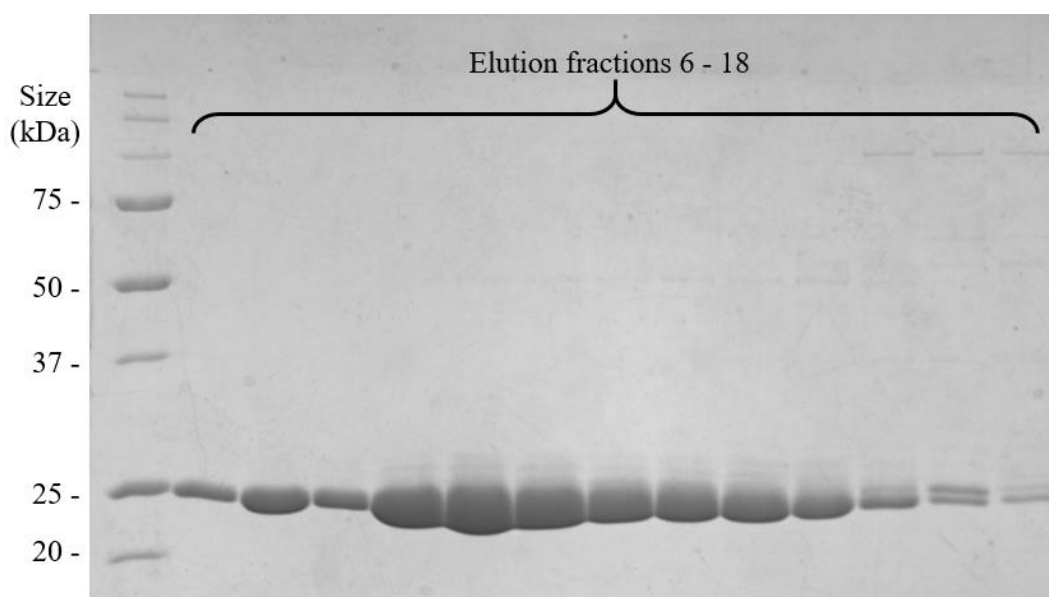
Figure 10: SDS-PAGE of anion exchange purification of NQO2.

Anion exchange purification was performed following TEV-protease digestion and dialysis into an appropriate buffer. Elution fractions 6-18 at 2 mL/min were yellow in colour, indicating presence of NQO2.

3.2.3.2   Addition of DTT at the FAD reconstitution step prevents dimerization due to disulfide bonds

The purification protocol for NQO2 requires denaturation and refolding in the presence of FAD, in order to fully reconstitute the enzyme with FAD rather than FMN (46). The results from the gel exclusion chromatography showed two peaks at the expected elution volume for NQO2 rather than one (**Figure 11, panel A**).
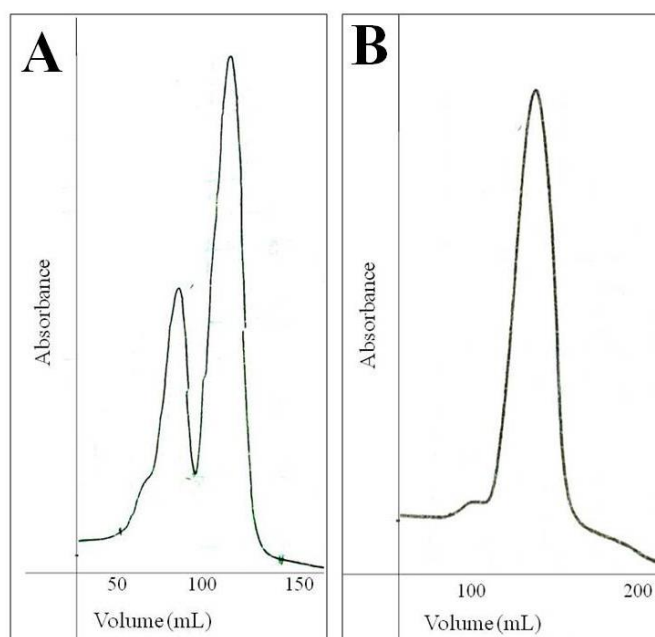
Figure 11: Preparative size-exclusion chromatography of NQO2, with and without reducing agent.

Panel A shows purification with no DTT used, while panel B shows purification with 10 mM DTT added into the guanidine-HCl denaturation step. Volume is calculated from the elution of void column volume.

Analysis of peak fractions by reducing SDS-PAGE indicated that both peaks contained only NQO2 (**Figure 12, panel A**). However, non-reducing SDS-PAGE (performed in the absence of β-mercaptoethanol) revealed that the fractions corresponding to the first of the two

34

peaks showed bands at both 26 kDa and 52 kDa (**Figure 12, panel B**). Native NQO2 is

naturally a dimer, however it does not contain any intermolecular disulfide bonds. Therefore,

the formation of disulfide bonds between two monomers is inappropriate for purification of

functional NQO2, and mis-folding may have occurred when the protein re-folded on the

column.
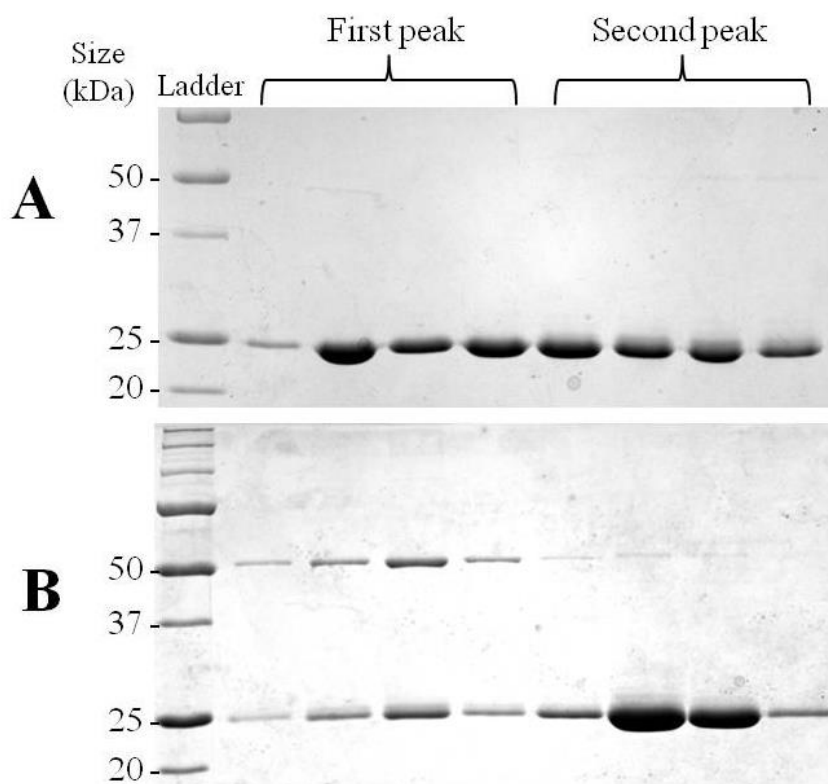
Figure 12: SDS-PAGE analysis of size-exclusion chromatography purification of NQO2.

In Panel A, the fractions were run on a reducing SDS-PAGE, while panel B is a non-reducing
gel. The first four fractions following the ladder in both gels correspond to the first of the two
NQO2 peaks seen on the chromatograph, while the last four correspond to the second, bigger
peak.

This may not be resolved by the addition of reducing agent after refolding, so the

protein eluted in the first peak was discarded and only the fractions from the second peak were

pooled and concentrated for later analysis. When the purification was repeated, 10 mM DTT was added into the guanidine-HCl denaturation step. The results from the size-exclusion chromatography from the second purification attempt showed only one peak (**Figure 11, panel B**) which was confirmed to be NQO2 by SDS-PAGE (not shown). The protein from the second purification was successfully used for analysis and crystallography. The addition of DTT was included in the purification process for NQO1, NQO2-trp and NQO2-qtp as well. An SDS-PAGE of the final products from each protein's purification shows that they are of acceptable purity for usage in enzymatic assays and crystallography (**Figure 13**). The total yield of purified protein was an average of 60 mg per litre of culture.
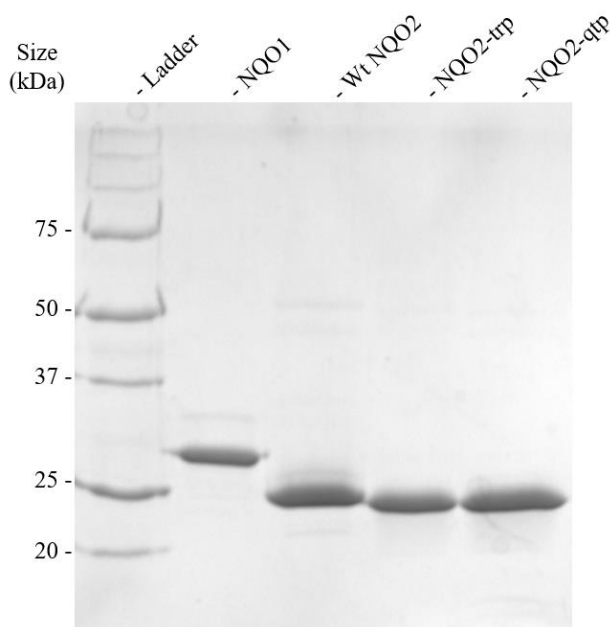
Figure 13: Purified NQO1, wildtype NQO2, NQO2-trp and NQO2-qtp.

An SDS-PAGE of the products of protein purification of NQO1, wildtype NQO2, NQO2-trp and NQO2-qtp.

3.2.4 CD scans of NQO1, NQO2 and mutants

Circular dichroism scans were conducted on NQO1, NQO2, NQO2-trp and NQO2-qtp (**Figure 14**). This was performed to observe any effects the mutations may have had on the general structure of NQO2, especially since a denaturation/refolding step was involved in the purification protocol. It also served to determine if the mutations changed the physical properties of NQO2 to approach those of NQO1. The data obtained showed ellipticity signal minima at 222 nm for all four proteins, as well as signal maxima at 195 nm, indicating significant helical content in the proteins. The highest to lowest maxima (195 nm) were NQO2-qtp, wildtype NQO2, NQO2-trp and NQO1. The highest to lowest minima (222 nm) were NQO1, wildtype NQO2, NQO2-trp and NQO2-qtp. The scans for all four proteins had the same general curve shape, any observable differences were in the amplitude of signal.
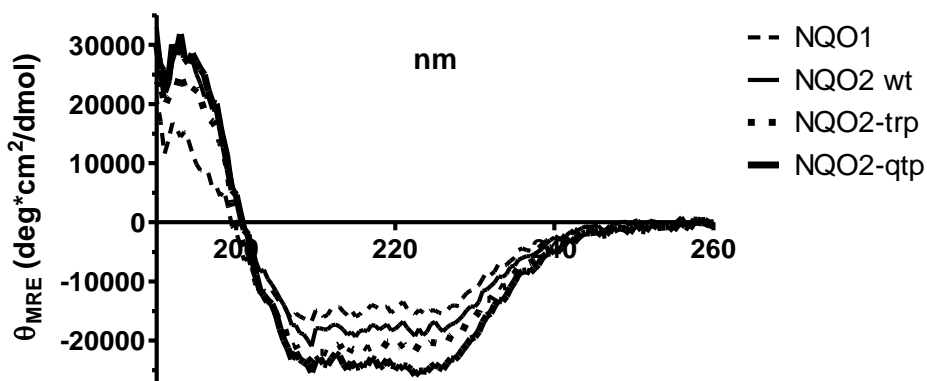
Figure 14: Circular dichroism scans of NQO1, NQO2, NQO2-trp and NQO2-qtp.

CD scans of the four proteins at 0.5 mg/mL in a 0.1 mm cuvette, ranging from 190 to 260 nm. All values were converted to mean residue ellipticity (Θ_{MRE}) which normalizes for concentration and size of the proteins.

Generally speaking, the CD scans of the mutants were within the same signal range and curve shape of the proteins, implying that the mutations did not significantly change the secondary structure of the protein. As for the specific differences in signal amplitude, there is a trend in the intensity of signal across NQO1 and the mutants. For example, the quintuple mutant possesses both the strongest maxima and minima, while NQO1 possesses the weakest strength signal. Across the two mutants and NQO1, the differences in signal intensity at the maxima and minima stays consistent. This implies that the only difference between these three proteins scans is signal strength. This observation can be explained by a margin of error in protein concentration, since a higher concentration of protein correlates to larger signal and vice versa. Overall, these spectra indicate that all the proteins are well folded.

3.2.5   Thermal denaturation curves of NQO1, NQO2 and mutants

Thermal denaturation curves were measured for NQO1, wildtype NQO2, NQO2-trp and NQO2-qtp using circular dichroism (**Figure 15**) in order to determine if the mutations had an effect on the thermostability of NQO2. The melting temperature (T_m) calculated from these curves for NQO1, wildtype NQO2, NQO2-trp and NQO2-qtp were 54.10, 75.05, 71.68 and 64.24 °C respectively. The most thermostable protein is wildtype NQO2, followed by NQO2-trp, NQO2-qtp and NQO1. The melting curves have sigmoidal shape indicating co-operative unfolding of the protein subunits. The results show that NQO1 is significantly less stable than NQO2. The triple and quintuple mutant were less stable than NQO2, getting closer to the melting temperature to that of NQO1.
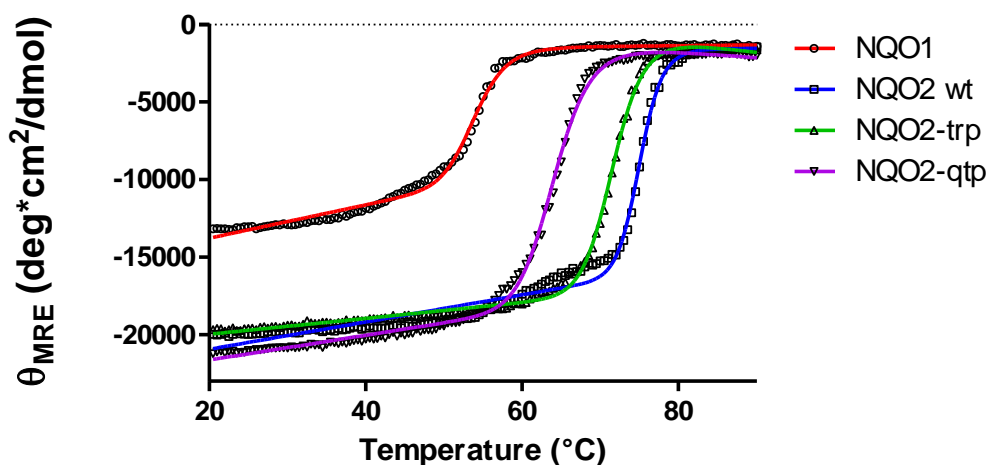
Figure 15: Thermal denaturation curves measured using circular dichroism for NQO1, wildtype NQO2, NQO2-trp and NQO2-qtp.

The temperature was increased from 20 to 90° C, and the signal was measured at 220 nm. All values were converted to mean residue ellipticity (Θ_{MRE}) which normalizes for concentration and size of the proteins

3.2.6   Enzyme kinetics measuring the effect of the mutations on NADH-driven mechanism

Following the purification of the mutants, enzyme kinetic assays were conducted as key experiments for this project, to determine if the protein's catalytic rates while utilizing NADH were affected by the mutations. I have performed these experiments on the four proteins (NQO1, NQO2, NQO2-trp and NQO2-qtp) using NADH, and paved the way for future kinetic analysis using NRH. The dye 3-(4,5-dimethylthiazol-2-yl)-2,5-diphenyltetrazolium bromide (MTT) was used as an indicator of enzyme activity as in previous methods with NQO1 and NQO2 (2, 17, 46, 53, 54). The assay combines a constant amount of protein, menadione and MTT alongside variable amounts of NADH into the buffer to obtain the catalytic rates of reaction. The protein utilizes NADH to reduce the quinone substrate (menadione) which

subsequently reduces the MTT dye in a non-catalyzed reaction. Upon reduction, the absorbance of MTT changes drastically which can be measured at 610 nm with an extinction coefficient of $11.3 \times 10^3 \, M^{-1} \, cm^{-1}$. The rate of change in absorbance is used to calculate the rate the enzyme is turning over substrate at that particular concentration of NADH, which can be used to obtain the catalytic efficiency of that protein as well as a Michaelis-Menten curve.

Since menadione can act as a substrate inhibitor of NQO2 at higher concentrations, the assay uses 10 µM menadione which was reported to be a low enough concentration that does not result in significant substrate inhibition (55). Both NQO1 and NQO2 can reduce menadione, therefore the reagents in the assay were consistent across the four proteins. The only variable between each protein's kinetic assay was the concentration of protein needed for a proper steady-state measurement. Keeping as many factors as possible consistent improves the reliability of the results when comparing the activities of the four proteins.

3.2.6.1   Kinetics of wildtype NQO1 using NADH as a cofactor

This assay was performed in order to ensure that the results were comparable to previously measured NQO1 K_m of 70 µM and k_{cat} of 515 s^{-1} (30,900 min^{-1}) using NADH as a cofactor (**Table 1**). Since the overall goal is to increase the catalytic rates of NQO2 with NADH to the rates seen from NQO1, the kinetic parameters obtained from this assay serve as a good baseline for comparison to the wildtype and mutant catalytic rates with NADH. The enzymatic rate of NQO1 using NADH as a cofactor and menadione as a substrate was measured using an MTT-dependent assay (**Figure 16**). The assay was performed in triplicate and the data were fitted to Michaelis-Menten kinetics equation using GraphPad Prism 4. Since this assay was performed to obtain relative kinetic parameters with NADH without determining the effect of

the two substrates individually, the reported parameters are apparent constants. The data fitting

reported a $K_{m(app)}$ of 291 µM with a 95% confidence interval of 191 to 389 µM, and a $k_{cat(app)}$ of

240 s^{-1} with a 95% confidence interval of 213 to 265 s^{-1}. The k_{cat} and K_m values obtained from

this experiment had a 2-fold and 4-fold difference, respectively, from the literature values. It is

worth noting that the previously quoted k_{cat} and K_m used a different assay to measure these

values, with DCIP as an indicator rather than MTT. While that may account for some of the

difference in the values obtained, the margin of error is not expected to be significant enough to

question the reliability of the data when comparing to the kinetic parameters observed for

wildtype NQO2 and the mutants. Since the values obtained for NQO1 are close to the literature

values and were performed under the same assay conditions as wildtype NQO2 and the

mutants, they provide a reliable basis for comparison and interpretation of the data.
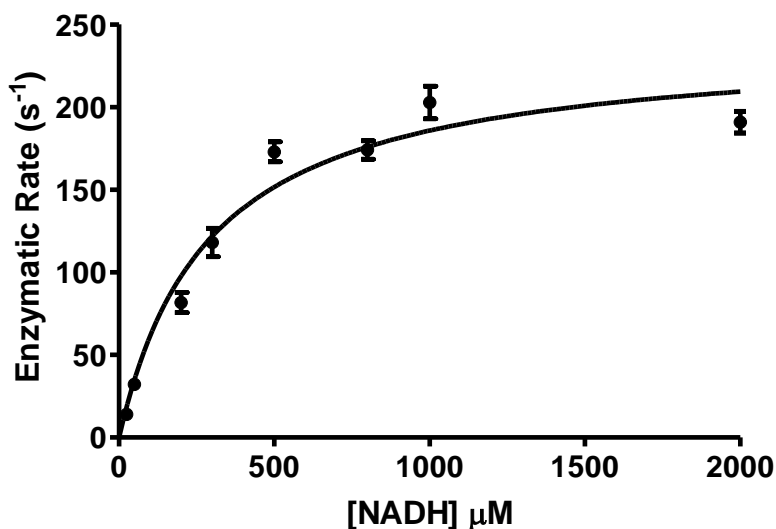
Figure 16: Enzymatic rate of NQO1 against NADH concentration.

The concentrations of MTT and menadione were kept constant while the concentration of
NADH was increased, and an increase in absorbance signifies MTT reduction. Performed in
triplicate.

3.2.6.2 Kinetics of wildtype NQO2 using NADH as a cofactor

This assay was performed in order to ensure that the results were comparable to previously measured NQO2 K_m of 330 µM and k_{cat} of 35 min^{-1} using NADH as a cofactor (**Table 1**). The enzymatic rate of NQO2 using NADH as a cofactor and menadione as a substrate was measured using the same MTT-dependent assay as in section 3.2.6.1 (**Figure 17**). By fitting the data to the Michaelis-Menten equation, the data reports a $K_{m(app)}$ of 1088 µM with a 95% confidence interval of 645 to 1530 µM, and a $k_{cat(app)}$ of 3.76 min^{-1} with a 95% confidence interval of 3.28 to 4.25 min^{-1}. The k_{cat} and K_m obtained from this experiment are within an order of magnitude from the aforementioned values published in literature, although they were further from the literature values than the parameters obtained using NQO1. As expected, the catalytic rates with respect to NADH are much higher in NQO1 than NQO2, since it is the native substrate of NQO1.
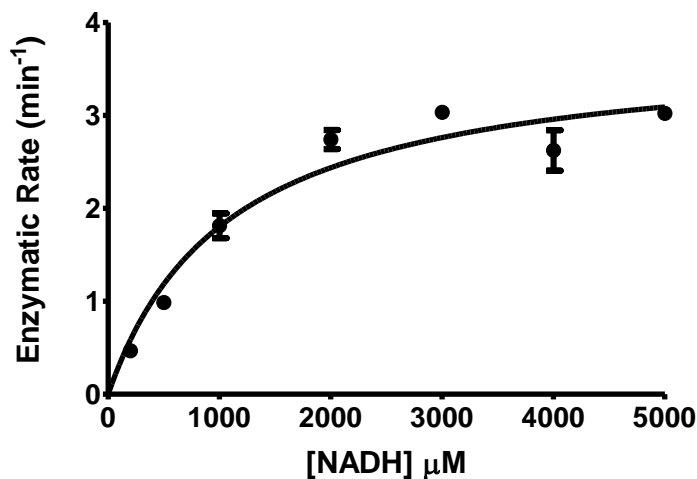
Figure 17: Enzymatic rate of wildtype NQO2 against NADH concentration.

The concentrations of MTT and menadione were kept constant while the concentration of NADH was increased. Performed in triplicate.

3.2.6.3 Kinetic analysis of wildtype NQO2 versus both mutants using NADH as a cofactor

In order to observe the effect the mutations had on the enzyme kinetics of NQO2, the same MTT-dependent assay that was performed on wildtype NQO2 was also performed on NQO2-trp and NQO2-qtp using NADH as a cofactor (**Figure 18).** The data from the above curve obtained for wildtype NQO2 is also included in the figure for comparison (shown in red data points). The full Michaelis-Menten curve for the enzymes could not be obtained due to the fact that there was no saturation observed for the mutants at very high concentrations of NADH. Although the wildtype enzymatic rates reached plateau by approximately 3 mM of NADH, the same assay with the mutants did not show saturation up to 10 mM. Attempting to raise the concentrations of NADH higher than 10 mM was not feasible due to highly rapid exhaustion of reagents available. It is important to mention that control tests were performed to ensure that there was no background reduction of the dye by individually eliminating each of the protein, menadione and NADH when running the assay. This determines if there was any direct reduction of the dye that resulted in background signal that could be mistaken for enzyme activity. There was no observable reduction of the dye when any of the protein, NADH, or menadione were not included in the assay (data not shown).

The fact that saturation with the mutants was not observed up to 10 mM of NADH was unexpected, considering that the mutants are shown to have higher enzymatic rates using NADH compared to the wildtype. This implies that the mutations may have had a mixed effect on the protein's catalytic properties by significantly both the $K_{m(app)}$ and $k_{cat(app)}$. Since saturation was not observed for the mutants, fitting to the Michaelis-Menten equation would not be reasonable due to very large uncertainties.
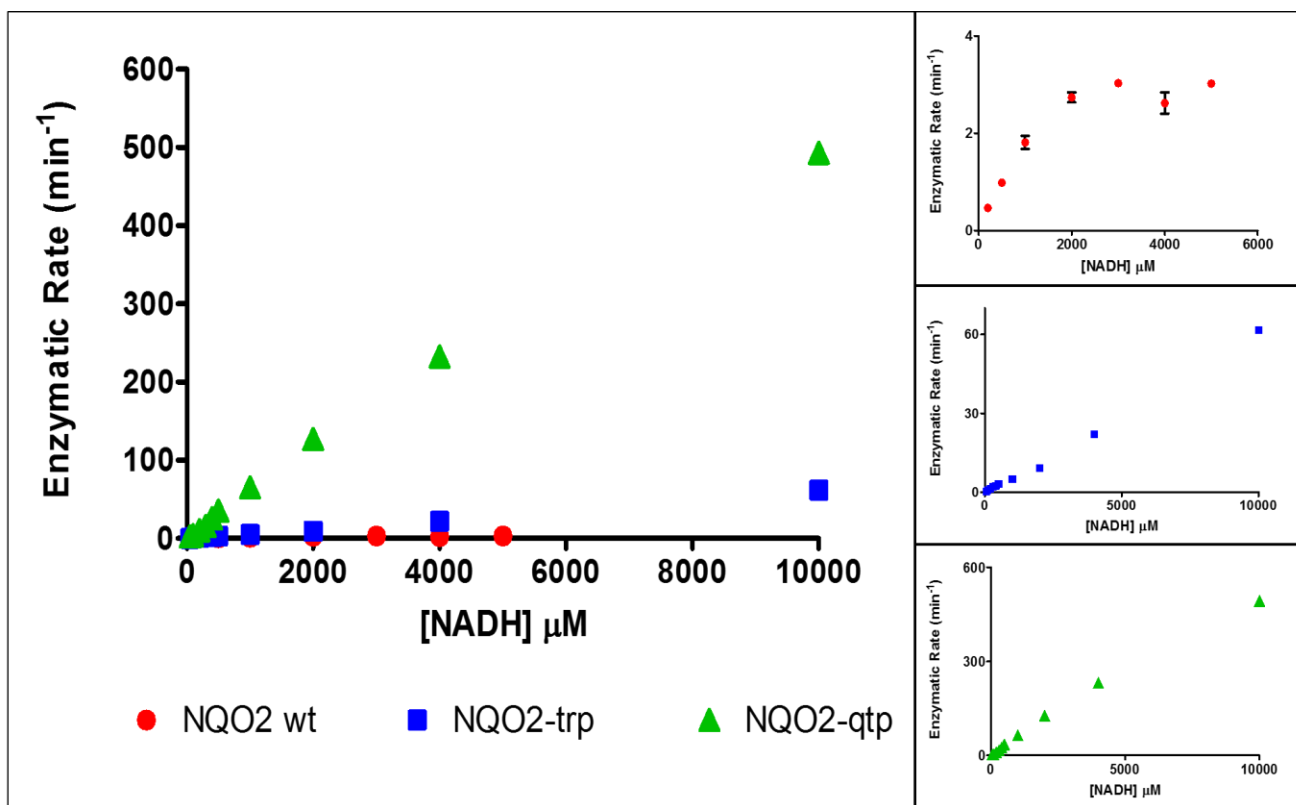
Figure 18: Enzymatic essay comparing the kinetics of wildtype NQO2, NQO2-trp and NQO2-qtp using NADH.

Very high concentrations of NADH (up to 10,000 µM) were used in an attempt to realize the full saturation curve for the mutants. The saturation curve obtained for wildtype NQO2 is included for comparison (red data points). Assay for both mutants was not performed in triplicate due to the amount of reagents and enzyme exhausted at high NADH concentrations. The three data curves are shown separately in the right column of panels to visualize each trend of data.

Since it was not possible to obtain the full Michaelis-Menten curve for the enzymes, the catalytic efficiency at lower concentrations of NADH was used to compare the effect of the mutants on the cofactor specificity of NQO2 (**Figure 19)**. The catalytic efficiency is defined by k_{cat}/K_m, and it can obtained by calculating the slope of the enzymatic rate at low concentrations of NADH – low enough that it is still linear without any saturation taking place. As seen in **Equation 2**, when the substrate concentration [S] is much lower than the K_m, the Michaelis-

Menten equation can be rewritten to estimate enzymatic rates as a liner function of substrate concentration [S] with a slope of total enzyme concentration $[E]_t$ multiplied by k_{cat}/K_m. V_{max} is the maximal rate of reaction, which equals the turnover number k_{cat} multiplied by $[E]_t$. The catalytic efficiency (k_{cat}/K_m) is a measure of how efficiently the protein can turn over substrate, expressed in concentration of substrate over time. The higher the catalytic efficiency, the better the enzyme turns over substrate.

Equation 2: Linear estimation of enzymatic rates at low substrate concentrations

$$Rate = V_{max} \cdot \frac{[S]}{K_m + [S]}$$

$$when \; [S] \ll K_m, \quad Rate \approx [E]_t \cdot {k_{cat}}/{K_m} \cdot [S]$$

The most important information needed from these kinetics experiments is a comparison of the effects of the mutations on the catalytic rates of the enzyme, therefore comparing the catalytic efficiencies of the proteins is a suitable analysis for the purpose of this project. The data were fit to a linear equation, and the catalytic efficiencies for the wildtype NQO2, NQO2-trp and NQO2-qtp were 13, 110 and 918 $M^{-1}s^{-1}$. The NQO2 quintuple mutant had a catalytic efficiency over 70-fold bigger than wildtype NQO2, which is an exciting result showing that the mutations have significantly improved the efficiency of the enzyme using NADH. The catalytic efficiency obtained for wildtype NQO2 through this method can be compared to the efficiency calculated through the kinetic parameters obtained from the full curve, since those were achievable for the wildtype (**Figure 17**). Dividing the $k_{cat(app)}$ by the $K_{m(app)}$ from the Michaelis-Menten curve fit yields a catalytic efficiency of 57.66 $M^{-1}s^{-1}$, which is within a 5-fold difference from 13 $M^{-1}s^{-1}$ that was calculated by the linear approximation method (**Figure 19**).

Considering the previously listed confidence interval of the parameters obtained from the Michaelis-Menten curve, the values are sufficiently close to each other to validate the linear approximation method of calculating the catalytic efficiency.
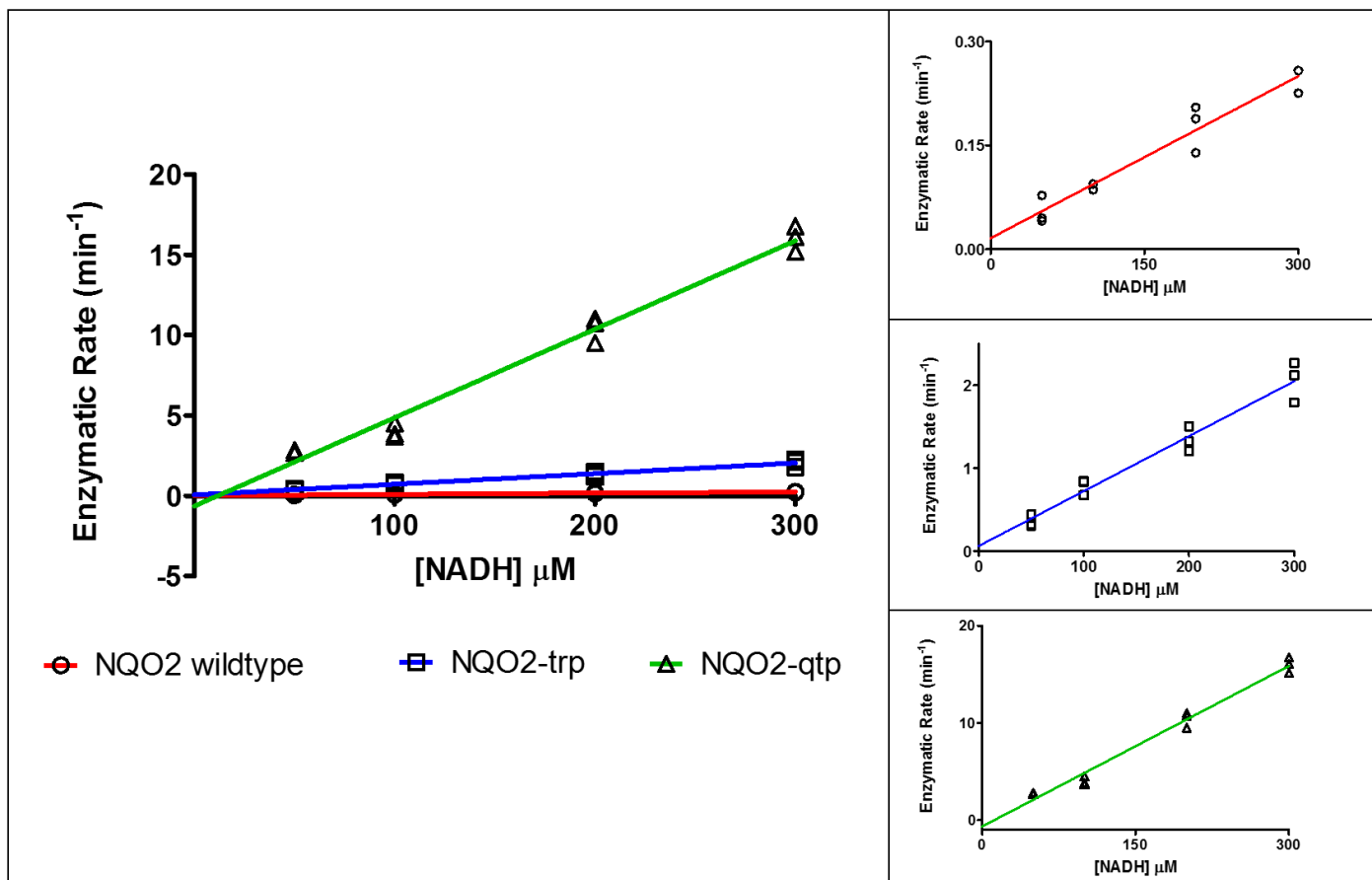
Figure 19: Enzyme kinetics comparing catalytic efficiency of wildtype NQO2, NQO2-trp and NQO2-qtp using NADH

MTT-dependent enzyme kinetics assay comparing the catalytic efficiency of NQO2 versus NQO2-trp and NQO2-qtp, using NADH as the cofactor and menadione as the substrate. Performed in triplicate.

The enzymatic assays revealed the exciting fact that substituting these residues had a pronounced effect on the cofactor specificity of NQO2 with NADH. The mutants, especially NQO2-qtp, had significantly higher catalytic efficiency with NADH compared to the wildtype.

This opens the door for performing the same kinetic analysis using NADPH and NRH. Most importantly, although there is still plenty of room for improvement and fine tuning of the mutant, the results are quite promising of an NQO2 that can be used *in vivo* to characterize the physiological role of the enzyme.

3.3   In silico and crystallography structural analysis of NQO2 and NQO1

In order to examine how NQO2 binds NRH, a structural comparison to other flavoenzymes which utilize NADH (including NQO1) has been quite informative. The initial reasoning for performing this comparison was to infer any potential shared binding site attributes amongst NQO1 and the other flavoenzymes that are responsible for their preference towards NADH, therefore helping illuminate what needs to be changed to make NQO2 specific to NADH. However, the structural comparison revealed that NQO2 and NQO1 have different binding stereochemistry altogether. An attempt at co-crystallization of NQO2 with NADH yielded discernible electron density for the nicotinamide moiety, which was useful for understanding how nicotinamide stacks onto the FAD molecule within the active site.

3.3.1   In silico comparison of NQO2 and NQO1 active site compared to related flavoenzymes

The electron transfer mechanism commonly used by NADH-utilizing flavoenzymes requires that the nicotinamide ring stacks onto the isoalloxazine ring of FAD, bringing the two reducing sites from each molecule in close proximity for the electron transfer to occur. Indeed, the majority of the enzyme structures which include both NAD and FAD from the Protein Data Bank (PDB) showed the two ring structures stacking together as such. PDB ID structures 1F3P,

1GEU, 2EQ7, 2NPX, 2RAB, 3CGD, 2YVG, 3GD4, and 4EMI (56–63) (**Table 4**) have been

superimposed by the isoalloxazine ring in order to compare how these proteins bind their

respective NAD molecules (**Figure 20**). The NAD molecules from these proteins bind at the

re-face of the isoalloxazine ring. Panel B adds the FAD molecules from NQO1 (yellow) and

NQO2 (orange) as well as the two proteins' backbone structures. In NQO1 and NQO2, the *re*-

face is buried within the protein, as seen in Panel B by the interference of a backbone loop from

both structures. In addition, the tail of the FAD molecule is projecting towards a different angle

in NQO1 and NQO2 in comparison with the FAD from the other protein structures. The fact

that the *re*-face is buried in NQO1 and NQO2 means that it is impossible to bind NADH at the

re-face as observed in all other flavoenzyme structures.

Table 4: List of proteins in the in silico superimposition with NQO2 and NQO1

1F3P	Ferrodoxin reductase
1GEU	Glutathione reductase
2NPX	NADH peroxidase
2RAB	Glutathione amide reductase
3CGD	CoA-disulfide reductase
2YVG	Ferrodoxin reductase (blue-semiquinone)
3GD4	Murin apoptosis-inducing factor
2EQ7	Lipoamide dehydrogynase
4EMI	Toluene dioxygenase reductase
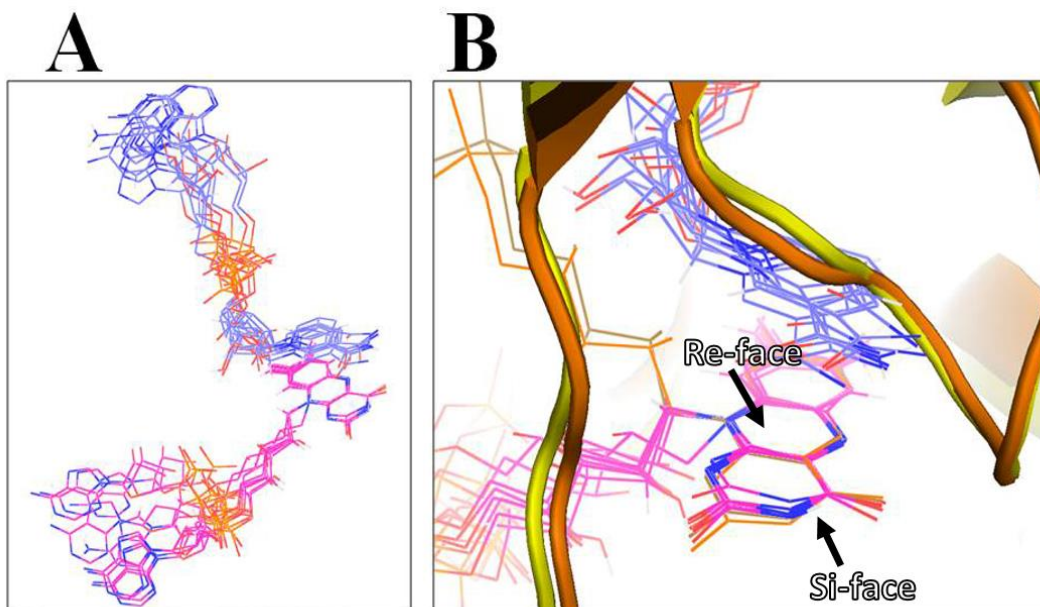
Figure 20: Steric interference of NQO2 and NQO1 backbone with consensus nicotinamide stacking position from other relevant protein structures

Panel A shows the FAD molecules (magenta carbons) and NAD molecules (blue carbons) stacking from protein structures 1F3P, 1GEU, 2NPX, 2EQ7, 2RAB, 3CGD, 2YVG, 3GD4, and 4EMI. All proteins were superimposed by the isoalloxazine ring of the FAD molecule. Panel B adds the FAD and backbones of NQO1 (yellow) and NQO2 (orange), superimposed onto the other structures by the isoalloxazine ring of the FAD molecule. The *re*-face and *si*-face of FAD are indicated, with the *re*-face facing upwards.

3.3.2   Crystallization of NQO2 with NADH soak

Part of the mystery surrounding the cofactor specificity of NQO2 was whether or not it has the ability to bind and utilize NADH. NRH is known as the primary cofactor for NQO2 but previous work reported a weak K_m of approximately 330 µM using NADH (**Table 1**). This, alongside the kinetic analysis from this project, supports that NQO2 can indeed bind and utilize NADH. This led to attempting crystallization of NQO2 with NADH. Our hypothesis was that NQO2 may be binding NADH and staying in the bound state for a prolonged period, making substrate turnover inefficient. If this were the case, obtaining a crystal structure of that

49

intermediate stage would be feasible. Therefore, NQO2 crystals were soaked in a cryoprotectant

solution containing 10 mM NADH. Upon soaking, the crystals were observed to turn from

yellow to colourless, and stayed colourless for a minimum of 5 minutes. This may imply that

NQO2 is being reduced and staying reduced for that duration. The soaked crystals were

immediately frozen and mounted for data collection. The full crystal structure was visualized in

PyMOL (**Figure 21**). The RMSD of the crystal structure backbone compared with NQO2

structure 1QR2 is 0.207 Å, which implies almost identical backbone structure.
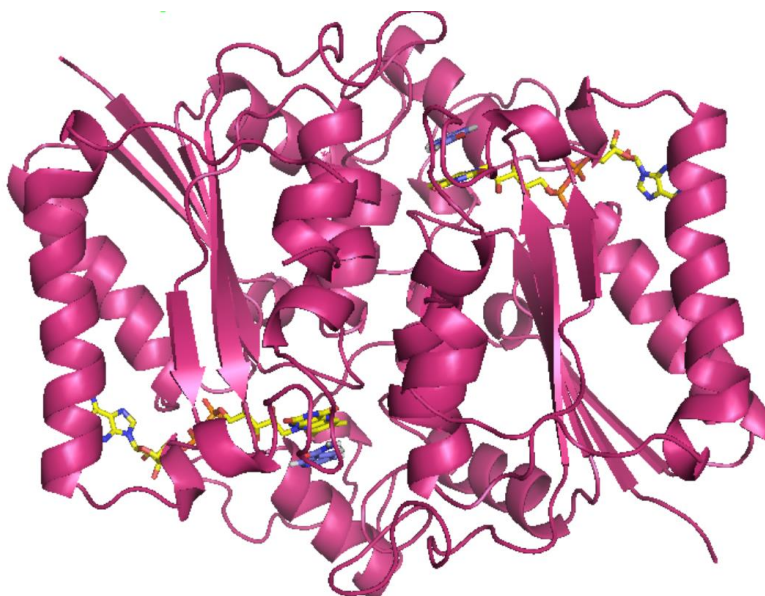
Figure 21: Full crystal structure obtained from crystallization of NQO2 with NADH soak and refinement with nicotinamide

Cartoon-representation of NQO2 in magenta with the FAD molecules shown with yellow carbons, and the refined nicotinamide in blue. The structure was refined using PHENIX with nicotinamide in the active site.

Electron density within the binding site was observed, which was smaller than an

NADH molecule and about the size of the nicotinamide moiety (**Figure 22**). Upon refinement

with nicotinamide, it became apparent that this electron density was a good match. Data and

refinement statistics can be found in **Table 5**. There was no density observed resembling the rest of the NADH molecule. This could mean that either the rest of the NADH molecule adopts a more erratic and less consensus sequence leading to poor electron density, or it could be indicating that the molecule has degraded where only the nicotinamide moiety is present in the active site. Three hydrogen bonds are present between the refined nicotinamide moiety, N161 from NQO2, and a water molecule in the active site (**Figure 23**). The presence of hydrogen bonds was determined by a bond length of 3.0 Å or less between the participating molecules. These interactions support that the refined nicotinamide molecule is situated in an optimal binding position within the enzyme active site, and accurately represents how the nicotinamide moiety stacks onto the FAD in NQO2.
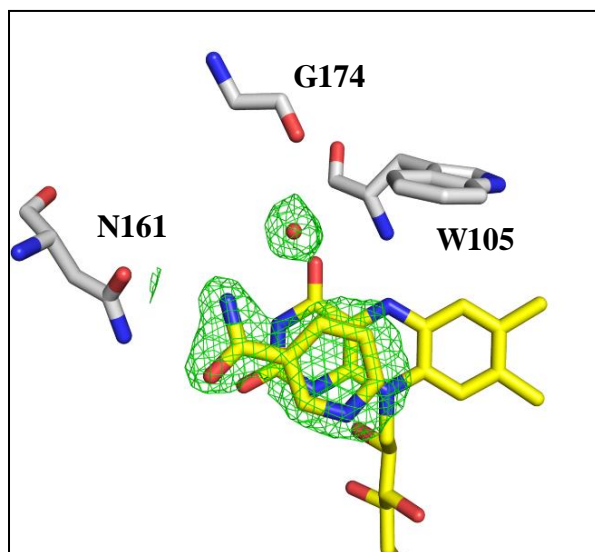
Figure 22: Electron density from NQO2 crystal soak in 50 mM NADH

Electron density from the F_o-F_c observed above the isoalloxazine ring within the binding site of NQO2 after soak in cryoprotectant containing 50 mM NADH. Nicotinamide was refined within this structure using PHENIX. Residues in close proximity are labelled with 1-letter abbreviations.
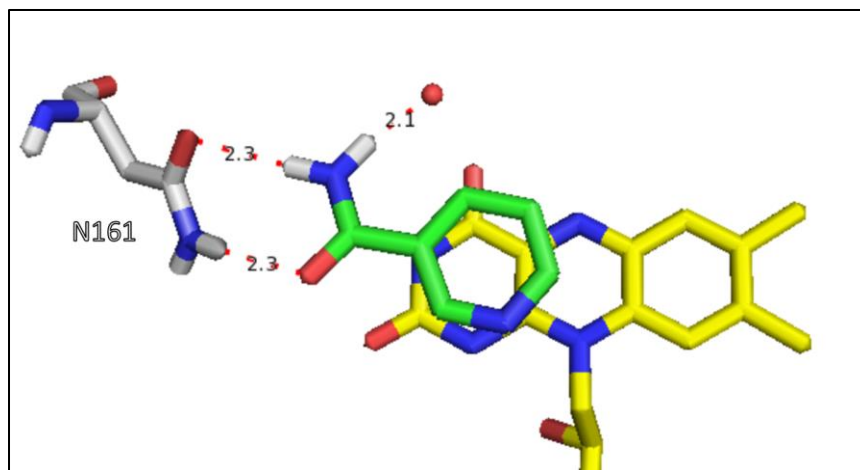
Figure 23: Hydrogen bonding of refined nicotinamide moiety with N161 and water in NQO2 active site.

Hydrogen bonds between the refined nicotinamide moiety (green carbons), N161 and water molecule in the NQO2 active site. The co-enzyme FAD is shown with yellow carbons. Taken from the crystal structure obtained from co-crystallization of NQO2 with NADH. Bond distance shown in Angstroms. Bond lengths measured and illustrated in PyMOL (64).

Table 5: Crystallographic data collection and refinement statistics

Crystal	NQO2-NADH
Ligand	NADH
Wavelength (Å)	1.5481
Space Group	$P2_12_12_1$
Unit Cell Dimensions (Ǎ)	56.19, 83.35, 106.37
Resolution (Å)	17.1 – 2.2
[a]R_{sym}	0.113 (0.471)
[a]$I/\sigma(I)$	14.4 (4.8)
Completeness	99.7 (100.0)
Multiplicity	7.1 (7.0)
Unique Reflections	25988
R_{work}/R_{free}	0.1673/0.2009
Ramachandran Plot[b] (%)	
Most Favoured	95.6
Generously Allowed	3.3
Disallowed	1.1
RMS Deviations	
Bond Lengths (Å)	0.008
Bond Angles (deg)	1.114
Mean A.D.P. values (Å^2)	
Protein	27.9
Solvent	30.0

[a]Values in parentheses refer to the highest resolution shell.

[b]Ramachandran plot statistics were calculated using CCP4

Chapter 4 – Discussion

4.1   Summary of findings

The results of this project can be summarized into two major categories: the effects of the site-directed mutagenesis on the properties of NQO2 and its catalytic rates utilizing NADH; and a structural-based analysis that includes the *in silico* comparison of NQO2 to NQO1 and other flavoenzymes as well as co-crystallization of NQO2 with NADH.

After mutating the chosen residues within the active site of NQO2 to those corresponding residues found in NQO1, the enzyme kinetics assays showed that the mutations increased the specificity of NQO2 towards NADH. The triple mutant and the quintuple mutant had a high catalytic efficiency using NADH, with the quintuple mutant's effect being most significant at 70-fold higher compared to wildtype NQO2. This was a very exciting result as it signifies that the mutated residues play an important role in the cofactor specificity of NQO2. Interestingly, attempting to obtain the full saturation curve for the wildtype and mutants was not possible at feasible concentrations of NADH (up to 10,000 µM), a phenomenon only occurring with the mutants and not the wildtype. This suggests that the $K_{m(app)}$ and $k_{cat(app)}$ of the mutants are extremely high, which invites some speculation as to why this phenomenon was observed.

In order to determine whether the mutations had an effect on the physicochemical properties of NQO2, thermal denaturation curves were obtained for the triple and quintuple mutant as well as wildtype NQO2 and NQO1. The triple and quintuple mutant had lower melting temperatures compared to wildtype NQO2, bringing them closer to the lowest melting temperature of NQO1.

These results imply that mutating these residues has shifted the stability of NQO2 closer to that of NQO1, which is not surprising considering that the residues substituted were the ones found in NQO1, and a hydrogen bond was removed in the process. This paves the way for future experiments analyzing the contribution of each of the individual residues to the thermal stability of NQO2.

The *in silico* comparison of NQO2 and NQO1 superimposed with other flavoenzymes that utilize NADH revealed that NQO1 and NQO2 bind their respective nicotinamide cofactor on the opposite face of the isoalloxazine ring of FAD, compared to other NADH-utilizing flavoenzymes. Considering that NQO2 and NQO1 have yet to be successfully co-crystallized with their respective cofactors (NRH and NAD(P)H), their differing stereochemistry may shed some light on why that task has proven more difficult than the other flavoenzymes. It also reinforces the importance of uncovering their binding specifics as it would reveal a new binding mode of nicotinamide cofactors onto the FAD co-enzyme.

An attempt at crystallization of NQO2 with NADH had rather interesting implications despite not being able to show the full electron density for NADH, and only that of the nicotinamide moiety. This observation suggests two different possibilities: the rest of the NADH molecule does not bind in a consensus binding position and is therefore unable to be visualized through crystallography, or that breakdown of the NADH molecule at the N-glycosidic bond has led to only nicotinamide being present in the binding site. This opens the door for future crystallization experiments to determine whether the full molecule was actually present in the binding site or if the molecule had degraded.

The results from this project illuminated some new facets to cofactor binding within NQO2. It opens the door for further examining the factors that influence the binding preference of NQO2, paving the way for future investigation and full characterization.

4.2   Structure and binding

Attempting to co-crystallize NQO2 with NADH yielded a discernible electron density for the nicotinamide moiety within the binding site, but no density resembling the rest of the NADH molecule (**Figure 22**). Observing the nicotinamide stacked upon the isoalloxazine of FAD supports that the mechanism of electron transfer from nicotinamide to FAD takes place as expected in NQO2. Although it is generally assumed that stacking of the N4 in nicotinamide upon N10 in FAD is how electron transfer occurs between a nicotinamide-based donor and the FAD in a flavoenzyme, it is helpful to observe this in NQO2 since it was seen in the *in silico* superimposition that NQO1 and NQO2 have a different mode of cofactor binding than other NADH utilizing flavoenzymes (**Figure 20**).

Since we have observed that the NQO2 crystals seem to remain in a reduced state for a prolonged period upon soaking in NADH (indicated by a change of colour in the crystals from yellow to colourless, and remaining colourless for over 5 minutes) this may be due to the NADH staying within the NQO2 active site for an extended period. It is unclear whether the reason NQO2 cannot efficiently use NADH is due to a low rate of electron transfer to FAD (e.g. due to non-optimal binding) or if it is due to a low release rate of NADH from the active site None of the results obtained in this project have contradicted the hypothesis that NQO2 cannot utilize NADH efficiently due to prolonged binding of the cofactor, rendering it overall inefficient. Therefore, it is plausible that this is the answer to the question of what determines

the cofactor preference of NQO2 for NRH over NADH. However, it is also possible that this observation is caused by exchange of oxidized NAD with NADH in solution, refreshing the reduced state of the protein until the NADH in the soaking solution is depleted. In order to examine whether this phenomenon is truly due to extended binding of NADH within the active site of NQO2, future assays on the binding kinetics of NQO2 must be pursued.

The fact that we did not observe the rest of the NADH molecule in the structure from the co-crystallization experiment suggests two possibilities: One being that the rest of the NADH molecule bound within NQO2 does not assume a consensus binding position, since 3D mapping through crystallography relies on ordered structure throughout the unit cell in the crystal. If the rest of the NADH molecule binds (or floats freely) in a disordered fashion within NQO2, it would be highly difficult to visualize it in the crystal structure. The second possibility is that mass breakdown occurred in the NADH molecule at the N-glycosidic bond connecting the nicotinamide to the ribose (and subsequently the rest of the NADH molecule). N-glycosidic bonds are known to be highly prone to hydrolysis in even slightly acidic environments. The NADH soaking/cryoprotectant solution used in this experiment was buffered at 7.5 pH which was expected to be an appropriate pH for the protein and NADH. However, repeating the experiment at pH 8 or 8.5 (at which NQO2 remains stable) may be worthwhile to determine whether the rest of the NADH molecule can be seen in the binding site. We do not expect the NADH purchased and used to contain high levels of free nicotinamide, however that could be another possible source for the lone nicotinamide moiety discerned in the binding site.

Since hydrogen bonding was observed between the refined nicotinamide molecule with N161 and water in the active site, this supports that the refined nicotinamide is in an optimal position for protein binding (**Figure 23**). Therefore, it is reasonable to assume that this structure

accurately represents the binding of nicotinamide derivatives in the NQO2 active site. Based on that assumption, an NADH molecule from the superimposition of the NADH-utilizing flavoenzymes was modelled into the NQO2 crystal structure obtained from the co-crystallization experiment, guided by the position of the refined nicotinamide moiety (**Figure 24**). Since the NADH molecules in the flavoenzyme superimposition were all shown to adopt a very similar extended conformation, any of them were considered representative of the conformation NADH prefers to adopt during protein binding (**Figure 20**). The nicotinamide moiety of the modelled NADH molecule was superimposed onto the refined nicotinamide within the NQO2 structure using PyMOL, and the nicotinamide-ribose bond was manually rotated to allow for better fit within the binding cavity (**Figure 24, panel A**). The manual adjustments needed to observe a plausible fit were minor; the original and rotated NADH are shown superimposed by their nicotinamide moieties for the sake of comparison (**Figure 24, panel B**). For better clarity on where the residues chosen for mutation lie in this proposed model, the five residues are highlighted and labelled (**Figure 24, panel C**). I propose this model as an estimation of NADH binding within the NQO2 active site, informed by the position of the nicotinamide that was observed in the co-crystallization experiment. The fact that minor adjustments were required to the extended conformation NADH seen in the other flavoenzyme structures makes this model promising of what occurs in the enzyme. The five residues chosen for mutation lie in close proximity to the adenosine diphosphate portion of NADH, which is where NADH differs from the native substrate for NQO2, NRH. It is plausible that these residues are interacting with that portion of NADH, and influencing its binding and dissociation rates within NQO2. Although it is unclear how these residues may be involved in the preference of NQO2 for NRH over NADH, this attempt at modelling NADH deems it unsurprising that

mutating these residues had a pronounced effect on the catalytic rates of NQO2 with NADH. It is possible that these residues provide favorable interactions with NADH, which increases its dissociation rate within NQO2 and hinders the turnover efficiency of the enzyme. This logic is in line with the effects on catalytic efficiencies observed from substituting these residues in the mutant proteins.
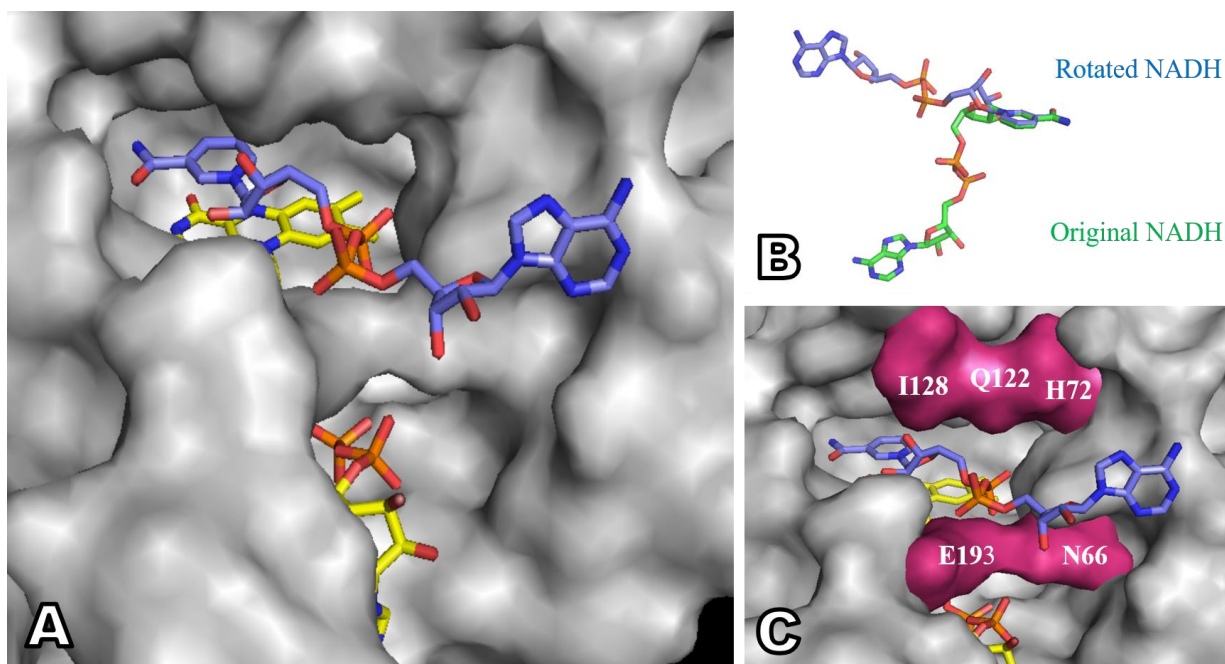
Figure 24: Representative NADH modelled into NQO2 structure obtained from co-crystallization with NADH

A representative NADH molecule taken from previously obtained NADH-bound flavoenzyme structure was modelled into the NQO2 crystal structure refined with nicotinamide. The nicotinamide moiety of NADH was superimposed onto the refined nicotinamide, and nicotinamide was omitted for clarity. The ribose-nicotinamide bond in NADH was manually rotated using PyMOL for a better fit in the nicotinamide cavity, as shown in Panel A (NADH with blue carbons, FAD co-enzyme shown in yellow carbons). Panel B shows a comparison of the original NADH molecule and the rotated NADH, superimposed by the nicotinamide moiety. Panel C shows the same modelled NADH within the NQO2 binding site as in Panel A, but with the five residues chosen for mutation highlighted in magenta and individually labelled.

4.3   Mutations and their effect on NQO2

4.3.1   Physicochemical changes caused by the mutations

Upon creating and purifying the NQO2 mutants, CD scans and denaturation curves were obtained in order to determine if the mutations had significantly changed the physicochemical properties of NQO2. Since one of the goals of using site-directed mutagenesis was to avoid making any major changes to the shape of the protein, ideally we wanted to see relatively little change in the properties of NQO2. If there were changes in physicochemical properties, we expected that they approximate those of NQO1 when compared to wildtype NQO2. Generally speaking, the CD scans of the mutants as well as the wildtype NQO2 and NQO1 had the same curve shape; a sign that there were no significant changes to the secondary structure of the protein (**Figure 14**). The shape of the curves was as expected of a predominantly helical protein.

As for the specific differences in signal amplitude, there was a trend in the intensity of signal across NQO1 and the mutants. For example, the quintuple mutant possesses both the strongest maxima and minima in terms of signal, while NQO1 possesses the weakest strength signal. Across the two mutants and NQO1, the differences in signal intensity at the maxima and minima stays consistent. This implies that the only difference between these three proteins' scans is signal strength. This observation can be explained by a margin of error in protein concentration, since a higher concentration of protein correlates to larger signal. Although stock solutions of the proteins were carefully measured by Bradford assay in triplicate, it is possible that some margin of error was introduced when diluting the proteins to the same concentration.

This may also explain why NQO1 has weaker signal strength that that of wildtype NQO2, since it is expected that their similar helical content would result in similar 195 and 220 nm signal.

On the contrary, the wildtype NQO2 somewhat disrupts this trend by having a relatively strong signal at 195 nm that is very close to that of the quintuple mutant, but its signal at 220 nm is weaker and approaches that of NQO1. This inconsistency in signal strength may imply a difference in secondary structure rather than a concentration margin of error. However, while observing the specifics of these CD curves it is important to note that the 0.1 mm cuvette used in order to be able to discern a signal in the lower wavelength range will result in a weak overall signal that is susceptible to noise. Therefore it is best to use it as a qualitative analysis, as the signal noise may be responsible for the inconsistency in the curve belonging to NQO2. After all, the conversion of the raw data to mean residue ellipticity (Θ_{MRE}) will amplify experimental error. Therefore, it is reasonable to assume that the CD scans show that the mutants did not have any major structural effects to the protein, and the small discrepancies present can be accounted within margin of error.

The thermal denaturation assay on the four proteins revealed the mutations had a significant effect on the thermostability of NQO2. NQO2 had the highest melting temperature, followed by the triple mutant, quintuple mutant and NQO1 in decreasing order. The results show that the five mutations have contributed significantly to lowering the stability of NQO2, approximating that of NQO1. This is an unsurprising observation, since the residues substituted were those found in NQO1. Additionally, the E193G and N66Q mutations (included only in the quintuple mutant) result in the removal of a hydrogen bond, therefore lowering the thermostability of the folded state.

Previous literature reports melting temperature of 70 °C for NQO2 in HEPES-OH buffer (53). As for NQO1, the literature reports a melting temperature of 54.0 °C in sodium phosphate buffer, and two examples in HEPES-OH buffer reporting values of 56.0 and 55.7 °C (65, 66). The melting temperature of 54.1 °C obtained for NQO1 is very close to the literature values, especially the ones performed in the same buffer (sodium phosphate). However, the melting temperature obtained for wildtype NQO2 was higher than the literature value, 75.05 °C compared to 70 °C respectively. Comparing the melting temperatures of NQO1 and NQO2 from these results to the values found in literature, NQO1 was within 1 degree which is within an acceptable range to show the assay worked as expected. On the other hand, NQO2 had a melting temperature 5 degrees higher than that found in the literature value. It is important to note that the assay used to obtain the literature value for NQO2 included 1% w/v DMSO which was not used in this project. This may account for the discrepancy of the values between the observed T_m and the literature. The aforementioned reported values for NQO2 used a HEPES-OH buffer, pH 7.5 buffer compared to the 20 mM sodium phosphate, 100 mM NaCl, pH 7.5 used in this assay. Although both of those buffers are not expected to have an effect on thermostability, it can be seen from the literature values of NQO1 that the melting temperature observed in HEPES-OH buffer are different by up to 1.7 °C than in sodium phosphate. Repeating these experiments with the same buffer as the literature values is suggested in order to determine whether the difference in values for NQO2 is due to the assay conditions. Since all four proteins were subjected to the same assay, ultimately the assay compared the thermostability of the mutants to the wildtype proteins, and showed the effects of the mutations.

4.3.2　Kinetics of the mutants compared to wildtype NQO2 and NQO1

The kinetics experiments were the core of this project and they resulted in rather interesting observations. The most important is that the mutations increased the catalytic efficiency of the enzyme with NADH significantly, especially in the quintuple mutant (**Figure 19**). Since the quintuple mutant showed a 70-fold increase in catalytic efficiency (k_{cat}/K_m) compared to the wildtype, and a 9-fold increase compared to the triple mutant, it appears that the last two mutations (E193G, N66Q) had the most significant effect on increasing NADH turnover. These two residues form a hydrogen bond in NQO2 that is not present in NQO1, and they can be visualized as a "bridge" in proximity of the active site of NQO2 (**Figure 2**). These two residues seem to make the general area of the binding site of NQO2 more restricted than that of NQO1, therefore it is reasonable to suggest that they had the biggest effect on how the tail portion of NADH binds. The tail portion in this case refers to the part of NADH which differs from NRH, the adenosine diphosphate moiety (**Figure 4**). Another option to consider is that the dramatic increase in catalytic efficiency for the quintuple mutant could be due to synergistic effects by bringing all five mutations together, and not solely due to the N66Q, E193G mutations. It seems that the residues chosen for mutation play a large role in the preference of NQO2 for NADH, perhaps by sterically interfering with how NADH would normally lie within the binding site of NQO1 and making its binding simply inefficient. However, since we have observed that NQO2 does bind NADH, there is also the possibility that these residues facilitate certain binding positions for NADH within NQO2 that is inefficient for electron transfer. This could certainly help explain why NQO2 seems to stay reduced by NADH for an extended period of time, as we observed by the colour change of the NQO2 crystal upon soaking with

NADH. Perhaps NADH can act as a weak competitive inhibitor for NQO2, which needs to be overcome by a certain concentration of NRH in the cell. Exploring whether or not this is true could be performed with more kinetics experiments focused on inhibition of NQO2. Since this hypothesis also suggests that the reason the quintuple mutant was much more efficient because it eliminates prolonged binding of NADH in the binding site, a future experiment investigating this would be crystallization of the mutant and examining whether the extended reduced state with NADH occurs with the mutant as well. If it is true that the quintuple mutant eliminated prolonged binding of NADH, we would expect to see a rapid reversion of the colour of the crystal, if any change does occur. This can also be measured as a change in absorbance at 450 nm.

One thing to consider is that we did not observe the full molecule of NADH in the crystallization experiment, therefore we have not been able to ascertain whether the tail of the NADH molecule binds in a large spectrum of positions, or if the molecule broke down at the bond between the ribose and nicotinamide. If these residues mutated are indeed facilitating a specific binding position for NADH, we would expect to see NADH in that position within the crystal structure. Since that was not the case, we could hypothesize that these residues are facilitating a broad spectrum of NADH binding by prohibiting the optimal position for electron transfer that would be seen in NQO1.

When comparing the catalytic efficiency from the kinetics experiment to the literature values, there is a rather significant difference in the results obtained for wildtype NQO2. Previous work has cited a k_{cat}/K_m of 1,666 M^{-1} s^{-1} for NQO2 with NADH (23), which is over two orders of magnitude larger than the wildtype NQO2 value of 13 M^{-1} s^{-1} obtained from the kinetics experiment here. It is not fully clear why the experimental data did not

reproduce the literature value. However, a likely explanation would be the fact that the aforementioned study used a different assay to determine these values, using DCIP as an electron acceptor as opposed to menadione and MTT. In addition, the previous study did not mention what temperature the kinetics were performed. If it was at 37°C compared to our experiments at 20 °C, it is logical that the previous work reported significantly higher catalytic numbers. We can reasonably eliminate low enzyme activity as the reasons for this observation, since the purification was shown to be highly successful with no sign of misfolded protein or impurities. Repeating the experiments under the same assay and conditions as the aforementioned study would be a suitable pursuit for reproducing the literature values.

The fact that we were not able to observe saturation for the mutants compared to the wildtype NQO2 was unexpected. It raises the question of whether this is due to the $K_{m(app)}$ and $k_{cat(app)}$ rising significantly due to the mutations compared to the wildtype, or if there is an assay-related issue causing menadione and/or the MTT dye to continue getting reduced. Since the same assay was performed in the wildtype as well as NQO1 with no apparent problems in saturation, and there was no sign of non-enzymatic reduction observed in control tests, the first line of reasoning would not include an issue in the assay itself. For troubleshooting whether this is an assay-related phenomenon, the best course of action would be to repeat these experiments using a different kinetics assay. This could be done by using a different dye such as DCIP in order to measure reduction. If there are similar results observed with a different assay, this would show evidence that these observations are indeed due to the enzymes' catalytic rates. There is also the option of circumventing the complications arising from multi-step kinetics assays by performing a direct reduction assay

using stopped-flow techniques to measure the rate of reduction of the enzymes by the cofactor (NADH or NRH) itself. This method would give the most direct answer to whether the mutations have caused the enzyme to be more efficiently reduced by the cofactor, however it would not give the complete picture of the overall turnover rates of the enzyme.

If we assume the assay works as intended with the mutants then we can rationalize these high saturation levels by the fact that the $K_{m(app)}$ and $k_{cat(app)}$ values have significantly increased due to these mutations. If the k_{cat} increases that means that the enzyme turns over a higher number of substrate molecules per second. However if the K_m increases that may indicate lowered affinity for the substrate. Therefore, it is possible that these mutations have broadened the specificity of the NQO2 binding site by allowing it to turnover NADH more efficiently at the cost of its already weak affinity towards it. Another possibility for seeing higher $K_{m(app)}$ and $k_{cat(app)}$ for the mutants is if they resulted in an increase of the dissociation rate of NADH. This would increase the perceived $k_{cat(app)}$ due to the enzyme being refreshed for catalysis at a quicker rate, which may also result in a higher $K_{m(app)}$ value. Since we have seen some evidence towards prolonged binding of NADH within the binding site of NQO2, it is conceivable that the mutations have eliminated the molecular determinants facilitating prolonged binding of NADH (therefore resulting in higher rates of both cofactor dissociation and substrate turnover) without including the determinants of high affinity for NADH. This suggests that the mutations chosen have eliminated the aspects of NQO2 that cause prolonged binding of NADH and subsequent inefficiency utilizing it, but have not included the residues in NQO1 which facilitate its high affinity for NADH. It seems quite likely that these mutation have moved the mutant in the desired direction for shifting the cofactor specificity towards NADH. It is important to note that the k_{cat}/K_m I have observed

for NQO1 with NADH was approximately 8.24×10^5 M^{-1} s^{-1}, which is expected of an efficient protein using its native cofactor. This value is three orders of magnitude greater than the catalytic efficiency of the quintuple mutant (918 M^{-1} s^{-1}), which puts into perspective the fact that much more fine-tuning on the mutant NQO2 is needed to achieve catalytic efficiency with NADH similar to that of NQO1. If we wish to create an NQO2 that utilizes NADH with high affinity, there likely are more mutations needed to reach that goal.

If the dissociation rate of NAD from the active site is what causes NQO2 to utilize NADH inefficiently, this can be examined through analysis of its inhibition of NQO2 function. If NAD is also included in an enzymatic assay of NQO2 then its K_i can be determined, which could reveal whether it significantly inhibits the enzyme at higher concentrations. If NAD does indeed inhibit the protein then it would be by competitive inhibition, so the substrate used for inhibition enzymatic assays may be required to have comparably low affinity, such as NADH, as opposed to the native substrates for NQO2 (NRH or its analogues). Performing the assay with very low concentrations of NRH or an analogue may also produce a suitable analysis. There is a possibility that inhibition assays with NAD may not yield accurate results because it could be that NAD itself does not enter and inhibit the active site the same way as when it is already there after getting oxidized *in situ*. However, based on the assumptions derived from the collected data, an inhibition assay has the potential to reveal the real reason for why NQO2 is inefficient with NADH compared to NRH.

Tying these kinetics results to the proposed NADH binding model informed by the co-crystallization experiment with NADH (**Figure 24**), it is conceivable that the residues that were chosen for mutation participate in favorable interactions with the adenosine

diphosphate section of NADH. They are in close proximity to the adenosine diphosphate portion of the modelled NADH; their interactions with NADH could be causing its dissociation rate to be low, and hindering turnover efficiency. Since the catalytic rates of the quintuple mutant must be significantly higher before reaching levels comparative to NQO1, there is likely more residues involved in determining cofactor specificity that need to be targeted for future mutagenesis.

The results observed regarding the cofactor specificity of NQO2 with this site-directed mutagenesis approach was more effective than simply removing/adding the C-terminal portion found in NQO1. This confirms that the factors determining the two proteins' cofactor preference are subtle and residue specific. Future work on fine tuning the mutant should include a similar site-directed approach.

4.3.2.1   Alignment of NQO1 and NQO2 sequences showing conservation at the chosen mutation sites

Since the quintuple mutant had a significantly bigger effect on the catalytic efficiency of NQO2 than the triple mutant, it raised the question of which of the mutated residues plays the largest role in determining the cofactor specificity of NQO2. In an attempt to shed some light on this matter, a sequence alignment of 12 NQO2 and 17 NQO1 sequences from vertebrates was performed. This was done to observe whether levels of sequence conservation at all five residues sites aligns with these residues being important for enzyme function, and the changes in catalytic rates observed. This information is relevant for future fine tuning of the mutations made to observe larger effects on catalytic rates. Generally speaking, the alignment showed lower levels of conservation at those five residue sites in NQO1 (**Figure C- 1, Appendix C**) than the corresponding ones in NQO2 (**Figure C- 2,**

Appendix C). The alignment output summary for NQO1 and NQO2 alignment is shown in

Table 6 and **Table 7**, respectively. The top two residues by percent frequency are listed for

each site. In addition, the conservation score for each residue position is shown, which

assign a numerical value to the level of physicochemical properties conserved at that site. A

maximum score of 10 indicates conservation of all properties (67).

Table 6: Output summary from alignment of NQO1 sequences

NQO1					
Residue in H. sapien	**Q66**	**V72**	**G122**	**Y128**	**G193**
Top two residues by percent frequency	N 23%	G 35%	G 29%	Y 52%	G 64%
	K 17%	A 17%	Q 29 %	L 23%	R 11%
Conservation score	3	2	3	6	3

Table 7: Output summary from alignment of NQO2 sequences

NQO2					
Residue in H. sapien	**N66**	**H72**	**Q122**	**I128**	**E193**
Top two residues by percent frequency	N 84%	W 41%	Q 91%	F 58%	E 92%
	H, S 8%	H 33%	R 8 %	I 33%	D 8%
Conservation score	4	6	8	8	9

The highest levels of conservation was seen for E193 in NQO2, suggesting that this

residue is important for NQO2 function. Since this residue participates in a hydrogen bond

with N66 that is not present in NQO1, this supports that this hydrogen bond is a key player

in the cofactor specificity of NQO2. This is in line with the significant change in catalytic

rates observed by the quintuple mutant, where this H-bond was removed through the N66Q

and E193G mutations. Its H-bond partner N66 is not very well conserved in terms of its

physicochemical properties, however, despite whether the residue present at that site is N

(the vast majority), the two alternative residues seen can also participate in hydrogen

bonding (H and S). Therefore, if future mutants are created for the purpose of changing the cofactor preference of NQO2 to NADH, N66 and E193 should be included. I128 and Q122 also showed strong conservation in NQO2, and although NQO2-trp did not show as much of a pronounced effect on the catalytic efficiency as NQO2-qtp, these residues could be synergistically controlling the cofactor specificity of NQO2 alongside the E193-H66 H-bond. Deciding whether future mutation experiments should include Q122G and I128Y should be addressed by creating a double mutant that only contains E193G and N66Q and comparing that mutant's kinetics to those of the quintuple mutant. As for H72, it does not appear to be a relatively strong player in NQO2 function based on its levels of conservation.

It is also worthy of note that these five residue sites are poorly conserved in NQO1, which suggests that trying to change the cofactor specificity of NQO1 to NRH by performing the reverse mutations will not yield as much of a pronounced effect on its preference. It seems that throughout evolution NQO2 has diverged to contain these residues to direct its specificity towards NRH, but the residue sites themselves do not contribute much to NADH binding and specificity in NQO1.

4.4   Future research

The results from this project certainly help illuminate what is responsible for the preference of NQO2 for NRH over NADH, but there is still further analysis that must be done in order to achieve full characterization. Most importantly, the same kinetics experiments performed using NADH should be repeated with NRH (or a suitable analogue). Although the oxidized form (NR) can be readily obtained, the reduced form was not a commercially available product and needed to be synthesized in-house. Repeating the

kinetics experiments with NRH on the five proteins will fully reveal whether the mutations shifted the cofactor specificity of NQO2 from NRH to NADH, rather than simply increasing its efficiency using NADH. There is also the possibility that the mutations simply broadened the binding site's range of acceptable cofactors, as opposed to making it specific towards NADH. Performing the kinetics with NRH may reveal whether that is the case, if the efficiency with NRH remains close or even better than the wildtype. If the cofactor specificity shifted towards NADH, the expected results would be an overall lower catalytic efficiency using NRH in the mutants compared to the wildtype. If the mutant successfully shows a shift from NADH to NRH, then additional mutation sites can be included in order to attempt shifting the specificity further towards NADH, mimicking the catalytic efficiencies found in NQO1.

If a mutant that utilized NADH with high efficiency is successfully created, it is important to consider inhibition of the mutant protein by distinct NQO1 and NQO2 inhibitors. If the mutant NQO2 shows less inhibition by NQO2 inhibitors and higher inhibition by NQO1 inhibitors, this could indicate that the mutations are making the protein very similar to NQO1. Since the overarching goal is to open doors for *in vivo* studies surrounding the function of NQO2 in the cell, creating a protein that ultimately functions like NQO1 would counter these efforts. This can also be addressed by kinetic assays using unique substrates for NQO1 and NQO2 on the mutants, and determining how the mutations have changed the substrate specificity of the enzyme.

A mutant NQO2 that utilizes NADH efficiently while retaining NQO2 functionality would be a great tool for characterizing the role of NQO2 in the cell. If wildtype NQO2 is replaced by the mutant in a living cell, its levels of activity would be known since the

NAD(P)H levels in a cell are well characterized. The resulting phenotype, especially from fluctuating NAD(P)H levels can be analyzed with certainty that NQO2 is active. Since previous research has established connections of the proteins to anti-malarial drug mechanism and p53 pathway, cell lines that are used to manipulate these signaling pathways would be a good start.

4.5   Conclusion

The project's main goal was to shed some light on what elements affect the cofactor preference of NQO2 for NRH, a unique cofactor, over NADH. In doing so, the objective was to ultimately help address the signaling role of NQO2 in the cell, which seems to go beyond its detoxification pathway through reduction of quinones. The project's results showed that NQO2 and NQO1 have different binding stereochemistry than other flavoenzymes utilizing a nicotinamide-based cofactor, which reinforced the need to characterize their unique mode of binding. By attempting to shift the specificity of NQO2 from NRH to NADH through site-directed mutagenesis, the results show that the residues mutated significantly influence catalytic efficiency using NADH. This sets up a good foundation for further characterizing of the effect of the mutations on efficiency using NRH, and whether the mutations have partially or fully achieved the intended effect. The results also suggest that the mutations may have broadened the specificity of the enzyme as opposed to a shift in preference, which opens the door for further investigation and more potential mutations. Ultimately the project has resulted in forward momentum towards characterizing the molecular determinants of the cofactor specificity of NQO2, and creating a mutant NQO2 that can be utilized *in vivo* to determine its role in cell signaling.

References

1. Lind, C., Cadenas, E., Hochstein, P., and Ernster, L. (1990) DT-diaphorase: purification, properties, and function. *Methods Enzymol.* **186**, 287–301

2. Wu, K., Knox, R., Sun, X. Z., Joseph, P., Jaiswal, a K., Zhang, D., Deng, P. S., and Chen, S. (1997) Catalytic properties of NAD(P)H:quinone oxidoreductase-2 (NQO2), a dihydronicotinamide riboside dependent oxidoreductase. *Arch. Biochem. Biophys.* **347**, 221–228

3. Čènas, N., Anusevičius, Ž. ̌, Nivinskas, H., Misevičiene, L., and Šarlauskas, J. (2004) Structure-Activity Relationships in Two-Electron Reduction of Quinones. *Methods Enzymol.* **382**, 258–277

4. Vasiliou, V., Ross, D., and Nebert, D. W. (2006) Update of the NAD(P)H:quinone oxidoreductase (NQO) gene family. *Hum. Genomics*. **2**, 329–335

5. Deller, S., Macheroux, P., and Sollner, S. (2008) Flavin-dependent quinone reductases. *Cell. Mol. Life Sci.* **65**, 141–60

6. Krissinel, E., and Henrick, K. (2007) Inference of Macromolecular Assemblies from Crystalline State. *J. Mol. Biol.* **372**, 774–797

7. Foster, C. E., Bianchet, M. a., Talalay, P., Zhao, Q., and Amzel, L. M. (1999) Crystal structure of human quinone reductase type 2, a metalloflavoprotein. *Biochemistry*. **38**, 9881–9886

8. Faig, M., Bianchet, M. A., Talalay, P., Chen, S., Winski, S., Ross, D., and Amzel, L. M. (2000) Structures of recombinant human and mouse NAD(P)H:quinone oxidoreductases: species comparison and structural changes with substrate binding and release. *Proc. Natl. Acad. Sci. U. S. A.* **97**, 3177–82

9.   Delano, W. L. (2002) The PYMOL Molecular Graphics System. *Delano Sci.*

10.   Dinkova-Kostova, A. T., and Talalay, P. (2010) NAD(P)H:quinone acceptor oxidoreductase 1 (NQO1), a multifunctional antioxidant enzyme and exceptionally versatile cytoprotector. *Arch. Biochem. Biophys.* **501**, 116–123

11.   Long, D. J., Iskander, K., Gaikwad, A., Arin, M., Roop, D. R., Knox, R., Barrios, R., and Jaiswal, A. K. (2002) Disruption of dihydronicotinamide riboside:quinone oxidoreductase 2 (NQO2) leads to myeloid hyperplasia of bone marrow and decreased sensitivity to menadione toxicity. *J. Biol. Chem.* **277**, 46131–9

12.   Asher, G., Lotem, J., Cohen, B., Sachs, L., and Shaul, Y. (2001) Regulation of p53 stability and p53-dependent apoptosis by NADH quinone oxidoreductase 1. *Proc. Natl. Acad. Sci. U. S. A.* **98**, 1188–1193

13.   Khutornenko, A. a, Roudko, V. V, Chernyak, B. V, Vartapetian, A. B., Chumakov, P. M., and Evstafieva, A. G. (2010) Pyrimidine biosynthesis links mitochondrial respiration to the p53 pathway. *Proc. Natl. Acad. Sci. U. S. A.* **107**, 12828–12833

14.   Graves, P. R., Kwiek, J. J., Fadden, P., Ray, R., Hardeman, K., Coley, A. M., Foley, M., and Haystead, T. a J. (2002) Discovery of novel targets of quinoline drugs in the human purine binding proteome. *Mol. Pharmacol.* **62**, 1364–72

15.   Kim, E. L., Wu, R., Ru, A., Schmitz-salue, C., Warnecke, G., Bu, E., Pettkus, N., Speidel, D., Rohde, V., Schulz-schaeffer, W., Deppert, W., Giese, A., Lu, C., and Germany, R. W. (2010) Chloroquine activates the p53 pathway and induces apoptosis in human glioma cells. *Neuro. Oncol.*

16.   Chen, S., Wu, K., Zhang, D., Sherman, M., Knox, R., and Yang, C. S. (1999) Molecular characterization of binding of substrates and inhibitors to DT-diaphorase: combined approach involving site-directed mutagenesis, inhibitor-binding analysis, and computer

modeling. *Mol. Pharmacol.* **56**, 272–278

17.   Buryanovskyy, L., Fu, Y., Boyd, M., Ma, Y., Hsieh, T., Wu, J. M., and Zhang, Z. (2004) Crystal structure of quinone reductase 2 in complex with resveratrol. *Biochemistry*. **43**, 11417–26

18.   Joseph, P., Ii, D. J. L., Klein-szanto, A. J. P., and Jaiswal, A. K. (2000) Role of NAD (P) H : Quinone Oxidoreductase 1 (DT Diaphorase) in Protection against Quinone Toxicity. **60**, 207–214

19.   Leung, K. K. K., and Shilton, B. H. (2013) Chloroquine binding reveals flavin redox switch function of quinone reductase 2. *J. Biol. Chem.* **288**, 11242–51

20.   Liao, S., Dulaney, J. T., and Williams-Ashman, H. G. (1962) Purification and properties of a flavoprotein catalyzing the oxidation of reduced ribosyl nicotinamide. *J. Biol. Chem.* **237**, 2981–2987

21.   Baum, C. L., Selhub, J., and Rosenberg, I. H. (1982) The hydrolysis of nicotinamide adenine dinucleotide by brush border membranes of rat intestine. *Biochem. J.* **204**, 203–207

22.   Chen, S., Deng, P. S., Bailey, J. M., and Swiderek, K. M. (1994) A two-domain structure for the two subunits of NAD(P)H:quinone acceptor oxidoreductase. *Protein Sci.* **3**, 51–57

23.   Chen, S., Wu, K., and Knox, R. (2000) Structure-function studies of DT-diaphorase (NQO1) and NRH: quinone oxidoreductase (NQO2). *Free Radic. Biol. Med.* **29**, 276–84

24.   Liger, D., Graille, M., Zhou, C. Z., Leulliot, N., Quevillon-Cheruel, S., Blondeau, K., Janin, J., and Van Tilbeurgh, H. (2004) Crystal structure and functional characterization of yeast YLR011wp, an enzyme with NAD(P)H-FMN and ferric iron reductase activities. *J. Biol. Chem.* **279**, 34890–34897

25. Li, R., Bianchet, M. A., Talalay, P., and Amzel, L. M. (1995) The three-dimensional structure of NAD(P)H:quinone reductase, a flavoprotein involved in cancer chemoprotection and chemotherapy: mechanism of the two-electron reduction. *Proc. Natl. Acad. Sci. U. S. A.* **92**, 8846–50

26. Kwiek, J. J., Haystead, T. a J., and Rudolph, J. (2004) Kinetic Mechanism of Quinone Oxidoreductase 2 and Its Inhibition by the Antimalarial Quinolines. *Biochemistry*. **43**, 4538–4547

27. Tedeschi, G., Chen, S., and Massey, V. (1995) DT-diaphorase. Redox potential, steady-state, and rapid reaction studies

28. Sollner, S., Durchschlag, M., Fröhlich, K. U., and MacHeroux, P. (2009) The redox-sensing quinone reductase Lot6p acts as an inducer of yeast apoptosis. *FEMS Yeast Res.* **9**, 885–891

29. Iskander, K., Paquet, M., Brayton, C., and Jaiswal, A. K. (2004) Deficiency of NRH:quinone oxidoreductase 2 increases susceptibility to 7,12-dimethylbenz(a)anthracene and benzo(a)pyrene-induced skin carcinogenesis. *Cancer Res.* **64**, 5925–8

30. Radjendirane, V., Joseph, P., Lee, Y. H., Kimura, S., Klein-Szanto, A. J. P., Gonzalez, F. J., and Jaiswal, A. K. (1998) Disruption of the DT diaphorase (NQO1) gene in mice leads to increased menadione toxicity. *J. Biol. Chem.* **273**, 7382–7389

31. Celli, C. M., Tran, N., Knox, R., and Jaiswal, A. K. (2006) NRH:quinone oxidoreductase 2 (NQO2) catalyzes metabolic activation of quinones and anti-tumor drugs. *Biochem. Pharmacol.* **72**, 366–76

32. Xu, J., Patrick, B. A., and Jaiswal, A. K. (2013) NRH: Quinone oxidoreductase 2 (NQO2) protein competes with the 20 S proteasome to stabilize transcription factor

CCAAT enhancer-binding protein ?? (C/EBP??), leading to protection against ?? radiation-induced myeloproliferative disease. *J. Biol. Chem.* **288**, 34799–34808

33. Hochhaus, A., Druker, B., Sawyers, C., Guilhot, F., Schiffer, C. A., Cortes, J., Niederwieser, D. W., Gambacorti-passerini, C., Stone, R. M., Goldman, J., Fischer, T., Brien, S. G. O., Reiffers, J. J., Mone, M., Krahnke, T., Talpaz, M., and Kantarjian, H. M. (2008) Favorable long-term follow-up results over 6 years for response , survival , and safety with imatinib mesylate therapy in chronic-phase chronic myeloid leukemia after failure of interferon- ␣ treatment. **111**, 1039–1043

34. Adams, M. A., and Jia, Z. (2006) Modulator of Drug Activity B from Escherichia coli: Crystal Structure of a Prokaryotic Homologue of DT-diaphorase. *J. Mol. Biol.* **359**, 455–465

35. Ronquist, F., Teslenko, M., Van Der Mark, P., Ayres, D. L., Darling, A., Höhna, S., Larget, B., Liu, L., Suchard, M. A., and Huelsenbeck, J. P. (2012) Mrbayes 3.2: Efficient bayesian phylogenetic inference and model choice across a large model space. *Syst. Biol.* **61**, 539–542

36. Dereeper, A., Guignon, V., Blanc, G., Audic, S., Buffet, S., Chevenet, F., Dufayard, J. F., Guindon, S., Lefort, V., Lescot, M., Claverie, J. M., and Gascuel, O. (2008) Phylogeny.fr: robust phylogenetic analysis for the non-specialist. *Nucleic Acids Res.* 10.1093/nar/gkn180

37. Solomon, V. R., and Lee, H. (2009) Chloroquine and its analogs: A new promise of an old drug for effective and safe cancer therapies. *Eur. J. Pharmacol.* **625**, 220–233

38. Wallace, D. J., Gudsoorkar, V. S., Weisman, M. H., and Venuturupalli, S. R. (2012) New insights into mechanisms of therapeutic effects of antimalarial agents in SLE. *Nat. Rev. Rheumatol.* **8**, 522–533

39. Savarino, A., Boelaert, J. R., Cassone, A., Majori, G., and Cauda, R. (2003) Effects of chloroquine on viral infections: An old drug against today's diseases? *Lancet Infect. Dis.*

3, 722–727

40. Ying, W. (2008) NAD + /NADH and NADP + /NADPH in Cellular Functions and Cell Death: Regulation and Biological Consequences. *Antioxid. Redox Signal.* **10**, 179–206

41. Zhang, Q., Piston, D. W., and Goodman, R. H. (2002) Regulation of corepressor function by nuclear NADH. *Science*. **295**, 1895–1897

42. Veech, R. L., Eggleston, L. V, and Krebs, H. a (1969) The redox state of free nicotinamide-adenine dinucleotide phosphate in the cytoplasm of rat liver. *Biochem. J.* **115**, 609–619

43. Fraaije, M. W., and Mattevi, A. (2000) Flavoenzymes: Diverse catalysts with recurrent features. *Trends Biochem. Sci.* **25**, 126–132

44. Jaiswal, A. K. (1994) Human NAD (P) H : Quinone Oxidoreductase2: Gene structure, activity and tissue-specific expression. *J. Biol. Chem.* **269**, 14502–14508

45. Brehmer, D., Godl, K., Zech, B., Wissing, J., and Daub, H. (2004) Proteome-wide Identification of Cellulat Targets Affected by Bisindolylmaleimide-type Protein Kinase C Inhibitors. *Mol. Cell. Proteomics*. **3**, 490–500

46. Leung, K. K. K., Litchfield, D. W., and Shilton, B. H. (2012) Flavin adenine dinucleotide content of quinone reductase 2: Analysis and optimization for structure-function studies. *Anal. Biochem.* **420**, 84–89

47. Studier, F. W. (2005) Protein production by auto-induction in high-density shaking cultures. *Protein Expr. Purif.* **41**, 207–234

48.   Leslie, A. G. W., and Powell, H. R. (2007) Processing diffraction data with mosflm. *Springer*. **245**, 41–51

49.   Evans, P. (2006) Scaling and assessment of data quality. *Acta Crystallogr. D. Biol. Crystallogr.* **62**, 72–82

50.   Adams, P. D., Afonine, P. V, Bunkóczi, G., Chen, V. B., Davis, I. W., Echols, N., Headd, J. J., Hung, L.-W., Kapral, G. J., Grosse-Kunstleve, R. W., McCoy, A. J., Moriarty, N. W., Oeffner, R., Read, R. J., Richardson, D. C., Richardson, J. S., Terwilliger, T. C., and Zwart, P. H. (2010) PHENIX: a comprehensive Python-based system for macromolecular structure solution. *Acta Crystallogr. D. Biol. Crystallogr.* **66**, 213–21

51.   Swint, L., and Robertson, A. D. (1993) Thermodynamics of unfolding for turkey ovomucoid third domain: Thermal and chemical denaturation. *Protein Sci.* **2**, 2037–2049

52.   Santoro, M. M., and Bolen, D. W. (1988) Unfolding free energy changes determined by the linear extrapolation method. 1. Unfolding of phenylmethanesulfonyl alpha-chymotrypsin using different denaturants. *Biochemistry*. **27**, 8063–8

53.   Miettinen, T. P., and Björklund, M. (2014) NQO2 is a reactive oxygen species generating off-target for acetaminophen. *Mol. Pharm.* **11**, 4395–404

54.   Prestera, T., Prochaska, H. J., and Talalay, P. (1992) Inhibition of NAD(P)H:(quinone-acceptor) oxidoreductase by cibacron blue and related anthraquinone dyes: a structure-activity study. *Biochemistry*. **31**, 824–833

55.   Leung, K. K. K., and Shilton, B. H. (2015) Quinone reductase 2 is an adventitious target of protein kinase CK2 inhibitors TBBz (TBI) and DMAT. *Biochemistry*. **54**, 47–59

56.   Senda, T., Yamada, T., Sakurai, N., Kubota, M., Nishizaki, T., Masai, E., Fukuda, M.,

and Mitsuidagger, Y. (2000) Crystal structure of NADH-dependent ferredoxin reductase component in biphenyl dioxygenase. *J. Mol. Biol.* **304**, 397–410

57.   Mittl, P. R., Berry, a, Scrutton, N. S., Perham, R. N., and Schulz, G. E. (1994) Anatomy of an engineered NAD-binding site. *Protein Sci.* **3**, 1504–14

58.   Stehle, T., Claiborne, a, and Schulz, G. E. (1993) NADH binding site and catalysis of NADH peroxidase. *Eur. J. Biochem.* **211**, 221–6

59.   Van Petegem, F., De Vos, D., Savvides, S., Vergauwen, B., and Van Beeumen, J. (2007) Understanding nicotinamide dinucleotide cofactor and substrate specificity in class I flavoprotein disulfide oxidoreductases: crystallographic analysis of a glutathione amide reductase. *J. Mol. Biol.* **374**, 883–9

60.   Wallen, J. R., Paige, C., Mallett, T. C., and Karplus, P. A. (2010) Pyridine nucleotide complexes with Bacillus anthracis coenzyme A-disulfide reductase: A structural analysis of dual NAD(PH) specificity. **47**, 5182–5193

61.   Senda, M., Kishigami, S., Kimura, S., Fukuda, M., Ishida, T., and Senda, T. (2007) Molecular mechanism of the redox-dependent interaction between NADH-dependent ferredoxin reductase and Rieske-type [2Fe-2S] ferredoxin. *J. Mol. Biol.* **373**, 382–400

62.   Sevrioukova, I. F. (2009) Redox-linked conformational dynamics in apoptosis-inducing factor. *J. Mol. Biol.* **390**, 924–38

63.   Lin, T.-Y., Werther, T., Jeoung, J.-H., and Dobbek, H. (2012) Suppression of electron transfer to dioxygen by charge transfer and electron transfer complexes in the FAD-dependent reductase component of toluene dioxygenase. *J. Biol. Chem.* **287**, 38338–46

64.   DeLano, W. L. (2002) The PyMOL Molecular Graphics System. *Schrödinger LLC wwwpymolorg*. **Version 1.**, http://www.pymol.org

65. Lienhart, W.-D., Strandback, E., Gudipati, V., Koch, K., Binter, A., Uhl, M. K., Rantasa, D. M., Bourgeois, B., Madl, T., Zangger, K., Gruber, K., and Macheroux, P. (2017) Catalytic competence, structure and stability of the cancer-associated R139W variant of the human NAD(P)H:quinone oxidoreductase 1 (NQO1). *FEBS J.* **284**, 1233–1245

66. Medina-Carmona, E., Neira, J. L., Salido, E., Fuchs, J. E., Palomino-Morales, R., Timson, D. J., and Pey, A. L. (2017) Site-to-site interdomain communication may mediate different loss-of-function mechanisms in a cancer-associated NQO1 polymorphism. *Sci. Rep.* **7**, 44532

67. Livingstone, C. D., and Barton, G. J. (1993) Protein sequence alignments: A strategy for the hierarchical analysis of residue conservation. *Bioinformatics*. **9**, 745–756

68. Edgar, R. C. (2004) MUSCLE: Multiple sequence alignment with high accuracy and high throughput. *Nucleic Acids Res.* **32**, 1792–1797

69. Waterhouse, A. M., Procter, J. B., Martin, D. M. A., Clamp, M., and Barton, G. J. (2009) Jalview Version 2-A multiple sequence alignment editor and analysis workbench. *Bioinformatics*. **25**, 1189–1191

Appendix A: Alignment of wildtype human NQO1 and NQO2 sequences

```
Score = 5500
Length of alignment = 231
Sequence sp|P16083|NQO2_HUMAN :  1 - 231 (Sequence length = 231)
Sequence sp|P15559|NQO1_HUMAN :  1 - 274 (Sequence length = 274)

sp|P16083|NQO2_HUMAN MAGKKVLIVYAHQEPKSFNGSLKNVAVDELSRQGCTVTVSDLYAMNLEPRA
                     | |.. ||| || |  ||| ..|. |   |  ..|  |  ||||||||..|
sp|P15559|NQO1_HUMAN MVGRRALIVLAHSERTSFNYAMKEAAAAALKKKGWEVVESDLYAMNFNPII

sp|P16083|NQO2_HUMAN TDKDITGTLSNPEVFNYGVETHEAYKQRSLASDITDEQKKVREADLVIFQF
                     . ||||| | .| |.| |.  |||. |..|| ||||.  |||||||||
sp|P15559|NQO1_HUMAN SRKDITGKLKDPANFQYPAESVLAYKEGHLSPDIVAEQKKLEAADLVIFQF

sp|P16083|NQO2_HUMAN PLYWFSVPAILKGWMDRVLCQGFAFDIPGFYDSGLLQGKLALLSVTTGGTA
                     || ||.||||||||| .||.    ||.  .. || | ...| |.||.||||..
sp|P15559|NQO1_HUMAN PLQWFGVPAILKGWFERVFIGEFAYTYAAMYDKGPFRSKKAVLSITTGGSG

sp|P16083|NQO2_HUMAN EMYTKTGVNGDSRYFLWPLQHGTLHFCGFKVLAPQISFAPEIASEEERKGM
                     ||.  |..||   .|||.| | ||||||.|| ||....    .. . |  .
sp|P15559|NQO1_HUMAN SMYSLQGIHGDMNVILWPIQSGILHFCGFQVLEPQLTYSIGHTPADARIQI

sp|P16083|NQO2_HUMAN VAAWSQRLQTIWKEEPIPCTAHWHFGQ
                     . .| .||. || | |.  ..    |.
sp|P15559|NQO1_HUMAN LEGWKKRLENIWDETPLYFAPSSLFDL

Percentage ID = 46.75
```

Figure A- 1: Alignment of human NQO1 and NQO2 illustrating percent sequence identity

An alignment of human NQO2 and NQO1 sequences in Jalview showing the percent identity between the two proteins' amino acid sequence.

Appendix B: Alignment of wildtype NQO2 with sequenced NQO2-trp and NQO2-qtp after site-directed mutagenesis

```
wt              TTTCTAATCCTGAGGTTTTCAATTATGGAGTGGAAACCCACGAAGCCTACAAGCAAAGGT
Triple_mutant   TTTCTAATCCTGAGGTTTTCAATTATGGAGTGGAAACCGTCGAAGCCTACAAGCAAAGGT
                **************************************** :***********

wt              CTCTGGCTAGCGACATCACTGATGAGCAGAAAAAGGTTCGGGAGGCTGACCTAGTGATAT
Triple_mutant   CTCTGGCTAGCGACATCACTGATGAGCAGAAAAAGGTTCGGGAGGCTGACCTAGTGATAT
                ************************************************************

wt              TTCAGTTCCCGCTGTACTGGTTCAGCGTGCCGGCCATCCTGAAGGGCTGGATGGATAGGG
Triple_mutant   TTCAGTTCCCGCTGTACTGGTTCAGCGTGCCGGCCATCCTGAAGGGCTGGATGGATAGGG
                ************************************************************

wt              TGCTGTGCCAGGGCTTTGCCTTTGACATCCCAGGATTCTACGATTCCGGTTTGCTCCAGG
Triple_mutant   TGCTGTGCGGGGGCTTTGCCTTTGACTATCCAGGATTCTACGATTCCGGTTTGCTCCAGG
                ********.*******************::************************

wt              GTAAACTAGCGCTCCTTTCCGTAACCACGGGAGGCACGGCCGAGATGTACACGAAGACAG
Triple_mutant   GTAAACTAGCGCTCCTTTCCGTAACCACGGGAGGCACGGCCGAGATGTACACGAAGACAG
                ************************************************************

wt              GAGTCAATGGAGATTCTCGATACTTCCTGTGGCCACTCCAGCATGGCACATTACACTTCT
Triple_mutant   GAGTCAATGGAGATTCTCGATACTTCCTGTGGCCACTCCAGCATGGCACATTACACTTCT
                ************************************************************

wt              GTGGATTTAAAGTCCTTGCCCCTCAGATCAGCTTTGCTCCTGAAATTGCATCCGAAGAAG
Triple_mutant   GTGGATTTAAAGTCCTTGCCCCTCAGATCAGCTTTGCTCCTGAAATTGCATCCGAAGAAG
                ************************************************************
```

Figure B- 1: Alignment of wildtype NQO2 with sequenced triple mutant (NQO2-trp) after third round of site-directed mutagenesis

The mutations correspond to Q122G, H72V, I128Y, and were introduced using Quikchange™ mutagenesis protocol.

```
wt                TCTAATCCTGAGGTTTTCAATTATGGAGTGGAAACCCACGAAGCCTACAAGCAAAGGTCT
Quintuple_mutant  TCTAATCCTGAGGTTTTCCAGTATGGAGTGGAAACCGTCGAAGCCTACAAGCAAAGGTCT
                  *****************. * **************** :**********************

wt                CTGGCTAGCGACATCACTGATGAGCAGAAAAAGGTTCGGGAGGCTGACCTAGTGATATTT
Quintuple_mutant  CTGGCTAGCGACATCACTGATGAGCAGAAAAAGGTTCGGGAGGCTGACCTAGTGATATTT
                  ************************************************************

wt                CAGTTCCCGCTGTACTGGTTCAGCGTGCCGGCCATCCTGAAGGGCTGGATGGATAGGGTG
Quintuple_mutant  CAGTTCCCGCTGTACTGGTTCAGCGTGCCGGCCATCCTGAAGGGCTGGATGGATAGGGTG
                  ************************************************************

wt                CTGTGCCAGGGCTTTGCCTTTGACATCCCAGGATTCTACGATTCCGGTTTGCTCCAGGGT
Quintuple_mutant  CTGTGCGGGGGCTTTGCCTTTGACTATCCAGGATTCTACGATTCCGGTTTGCTCCAGGGT
                  ******. *****************::**********************************

wt                AAACTAGCGCTCCTTTCCGTAACCACGGGAGGCACGGCCGAGATGTACACGAAGACAGGA
Quintuple_mutant  AAACTAGCGCTCCTTTCCGTAACCACGGGAGGCACGGCCGAGATGTACACGAAGACAGGA
                  ************************************************************

wt                GTCAATGGAGATTCTCGATACTTCCTGTGGCCACTCCAGCATGGCACATTACACTTCTGT
Quintuple_mutant  GTCAATGGAGATTCTCGATACTTCCTGTGGCCACTCCAGCATGGCACATTACACTTCTGT
                  ************************************************************

wt                GGATTTAAAGTCCTTGCCCCTCAGATCAGCTTTGCTCCTGAAATTGCATCCGAAGAAGAA
Quintuple_mutant  GGATTTAAAGTCCTTGCCCCTCAGATCAGCTTTGCTCCTGGAATTGCATCCGAAGAAGAA
                  ****************************************. ******************
```

Figure B- 2: Alignment of wildtype NQO2 with sequenced quintuple mutant (NQO2-qtp) after final round of site-directed mutagenesis

The mutations correspond to Q122G, H72V, I128Y, E193G and N66Q and were introduced using Quikchange™ mutagenesis protocol.

84

Appendix C: Alignment of NQO1 and NQO2 sequences showing conservation and consensus residues at the chosen mutation sites
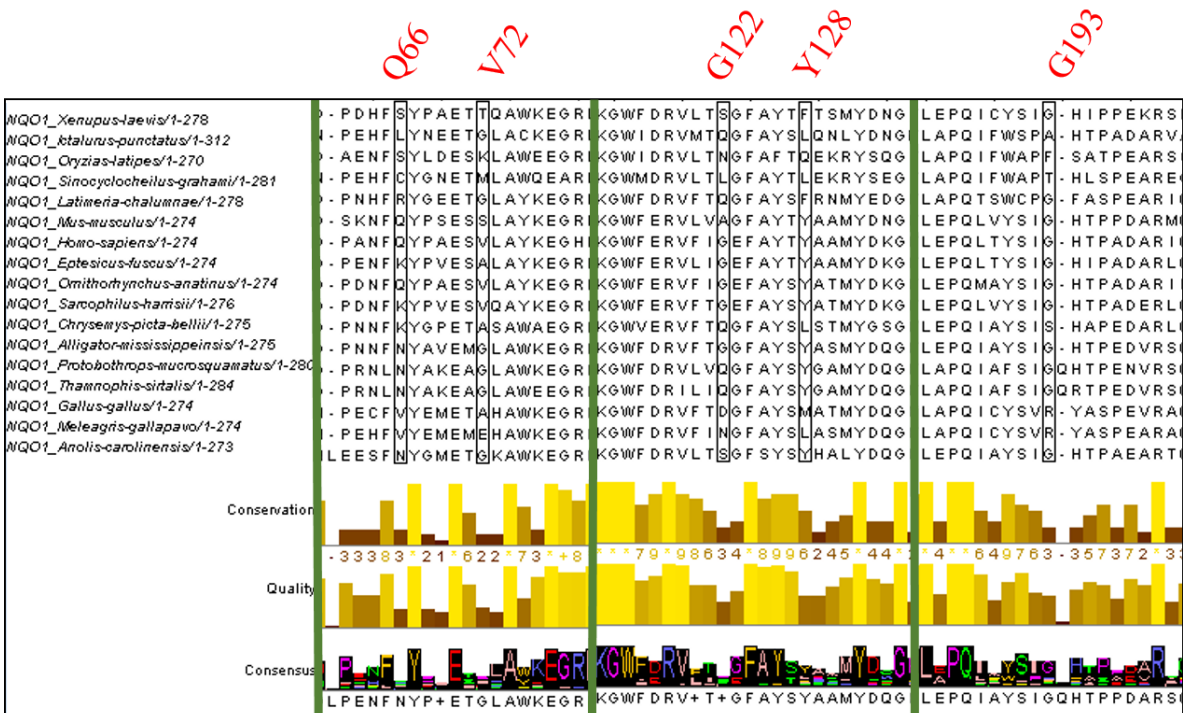

Figure C- 1: Alignment of NQO1 sequences showing conservation and consensus at the five chosen residue sites

Sequence alignment of 17 vertebrate NQO1 residues showing conservation and consensus sequence at the five residue sites corresponding to the chosen mutation sites from NQO2. Aligned with Muscle (68). Calculation of conservation score, consensus sequence and illustration performed in Jalview (69). Thick vertical green lines indicate hidden stretches of sequence.
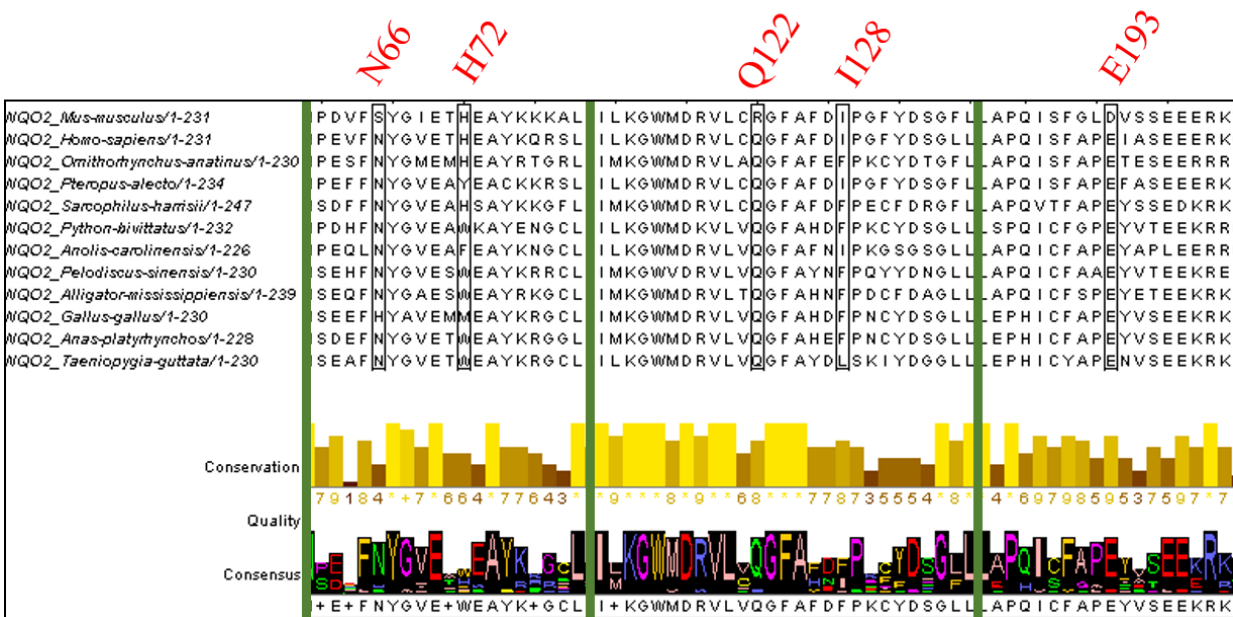
Figure C- 2: Alignment of NQO2 sequences showing conservation and consensus at the five chosen mutation sites

Sequence alignment of 12 vertebrate NQO2 residues showing conservation and consensus sequence at the five residue sites corresponding to the chosen mutation sites. Aligned with Muscle (68). Calculation of conservation score, consensus sequence and illustration performed Jalview (69). Thick vertical green lines indicate hidden stretches of sequence.

Curriculum Vitae

Name:	Al Massri, Shahed

Post-secondary Education and Degrees:

Master of Science Candidate - Biochemistry
Western University
London, ON, Canada
2015-Present

Bachelor of Medical Sciences - Honours Specialization in Biochemistry and Cell Biology
Western University
London, ON, Canada
2010-2015

Honours and Awards:

Western Graduate Research Scholarship
2015-2017

Dean's Honour List
2011-2015

Western Excellence Scholarship - Entrance with 90% average or higher
2010

Research Experience:

Master of Science Candidate - Biochemistry
Western University
London, ON, Canada
2015-2017

Biochemistry 4999E Project - Advanced Research in Biochemistry
Western University
London, ON, Canada
2014-2015

Undergraduate Honours Thesis Project
Western University
London, ON, Canada
2014

Related Work Experience

Teaching Assistant – 2nd and 4th year core Biochemistry courses
Western University
London, ON
2014-2016

Organics Lab Assistant – Student Internship
ALS Environmental
Waterloo, ON
2013-2014

Extracurricular: *Vice President (Academics sector)*
Western Biochemistry Club
London, ON, Canada
2014-2015

Volunteer Teacher and Fundraiser
MS Society
Waterloo, ON, Canada
2014